MODELLED TEMPERATURE-DEPENDENT EXCITABILITY BEHAVIOUR OF A GENERALISED HUMAN PERIPHERAL SENSORY NERVE FIBRE

Jacoba E. Smit[1], Tania Hanekom and Johan J. Hanekom

Department of Electrical, Electronic and Computer Engineering, University of Pretoria, Lynnwood Road, Pretoria, 0002, South Africa

Corresponding author: Prof Tania Hanekom

Department of Electrical, Electronic and Computer Engineering, University of Pretoria, Lynnwood Road, Pretoria, 0002, South Africa
Email: tania.hanekom@up.ac.za, Tel no: +27 12 420 2647, Fax no: +27 12 362 5000

Abstract

The objective of this study was to determine if a recently developed human Ranvier node model, which is based on a modified version of the Hodgkin-Huxley model, could predict the excitability behaviour in human peripheral sensory nerve fibres with diameters ranging from 5.0 – 15.0 μm. The Ranvier node model was extended to include a persistent sodium current and was incorporated into a generalised single cable nerve fibre model. Parameter temperature dependence was included. All calculations were performed in Matlab. Sensory nerve fibre excitability behaviour characteristics predicted by the new nerve fibre model at different temperatures and fibre diameters compared well with measured data. Absolute refractory periods deviated from measured data, while relative refractory periods were similar to measured data. Conduction velocities showed both fibre diameter and temperature dependence and were underestimated in fibres thinner than 12.5 μm. Calculated strength-duration time constants ranged from 128.5 μs to 183.0 μs at 37°C over the studied nerve fibre diameter range, with chronaxie times about 30% shorter than strength-duration time constants. Chronaxie times exhibited temperature dependence, with values overestimated by a factor 5 at temperatures lower than body temperature. Possible explanations include the deviated absolute refractory period trend and inclusion of a nodal strangulation relationship.

Keywords: *computational nerve fibre model, conduction velocity, chronaxie, refractory periods, persistent sodium current*

[1] *At the time of this research JE Smit was with the University of Pretoria and now resides at the Biophotonics group, CSIR National Laser Centre (NLC), Building 46, P.O. Box 395, Pretoria, 0001, South Africa*

ABBREVIATIONS

HH model, Hodgkin-Huxley model; ANF, Auditory nerve fibre; AP, Action potential; ARP, Absolute refractory period; RRP, Relative refractory period; GHK, Goldman-Hodgkin-Katz.

Introduction

Most studies centred on normal and pathological nerve fibre conduction in humans involve computational nerve fibre models. Originally physiologically based models have been based on *in vitro* recorded experimental data from squid (Hodgkin and Huxley 1952) and toad (Frankenhaeuser and Huxley 1964). Substantial efforts have since been made to develop models based on mammalian membrane dynamics, for both sensory and motor nerve fibres (see for example Chiu et al. 1979; Blight 1985; Schwarz and Eikhof 1987; Grill and Mortimer 1996; Bostock and Rothwell 1997; Stephanova et al. 2005, to name but a few). These models consist of a cable model describing the mechanism of action potential propagation along the nerve fibre. Integrated into this cable model is a membrane model, which describes the local action potential at the active nerve fibre sections (usually the nodes of Ranvier in myelinated nerve fibres). The main problem therefore is to decide upon the most applicable membrane model.

In the cochlear implant research field, computational models of the auditory nerve fibre (ANF) can be divided into physiologically based (Colombo and Parkins 1987; Frijns et al. 1994; Rubinstein 1995; Rattay et al. 2001; Rubinstein et al. 2001; Matsuoka et al. 2001; Morse and Evans 2003; Briaire and Frijns 2005) and phenomenological ANF models (Shannon 1989; Miller et al. 1999; Bruce et al. 1999; Zhang et al. 2001; Carlyon et al. 2005; Macherey et al. 2007). Even though the physical structure of human ANFs has been investigated (Nadol Jr 1988; Nadol Jr 1990; Nadol Jr et al. 1990; Zimmermann et al. 1995; Rosbe et al. 1996; Glueckert et al. 2005a; Glueckert et al. 2005b), the properties and types of ionic membrane currents of spiral ganglion cells have been characterised in murine (Mo et al.

2002; Reid et al. 2004; Hossain et al. 2005; Chen and Davis 2006) and guinea-pig (Bakondi et al. 2008), but not in human.

Human ANF models have been developed by Briaire et al. (2005; 2006) and Rattay et al. (2001). These models are partially based on human morphometric data, while the ionic current dynamics are still those of rat and squid respectively. A study comparing the applicability of the animal models of squid (Hodgkin and Huxley 1952), toad (Frankenhaeuser and Huxley 1964), rabbit (Chiu et al. 1979) and rat (Schwarz and Eikhof 1987) to predict human ANF excitation favours the Hodgkin-Huxley (HH) model, provided the nodal ion channel kinetics are accelerated tenfold (Rattay 1990; Rattay and Aberham 1993). This modified HH model shows improved human ANF response predictions by replacing the squid morphometric properties by those of human (Rattay et al. 2001).

Furthermore, the Briaire and Frijns (2005) model cannot fully account for the electrically evoked compound action potential (ECAP) morphology observed in humans, while Macherey et al. (2007) argue that the ion channels of the Rattay et al. (2001) model are not sufficient to account for non-monotonic excitation behaviour experimentally observed. They suggested that the voltage-gated ion channel currents that may explain these non-monotonic trends could be a combination of a slow potassium current and persistent sodium current (see for example the motor nerve fibre model by McIntyre et al. 2002). Hence, a more comprehensive computer model is needed, based on peripheral ANF characteristics. Since the human ANF is of the peripheral sensory type, the possibility exists that similar ionic membrane currents to those found in other peripheral sensory nerve fibres might be present. Ionic membrane current data from single human myelinated peripheral nerve fibres have been recorded by Reid et al. (1993; 1999), Scholz et al. (1993) and Schwarz et al. (1995), but only

the Schwarz et al. (1995) data have been used to develop human nerve fibre models (see for example models by Bostock and Rothwell 1997; and Wesselink et al. 1999). However, to date none of these data have been applied to simulate human ANFs.

The development of a general human peripheral sensory nerve fibre can hence serve as a step towards the development of a comprehensive human ANF model, until ionic membrane current data from human ANFs become available. Briaire and Frijns (2005) proposed a modification of their model with the ionic membrane dynamics of the Wesselink et al. (1999) model. Considering the better performance of the Rattay et al. (2001) model, the present study proposes the development of such an interim model of a human sensory nerve fibre, based on modification of the HH model to describe action potentials generated in a human Ranvier node. The model was developed in two phases. The first phase, namely the development of the Ranvier node model, was discussed in Smit (2008) and Smit et al. (2009). This article deals with the second phase, namely the development of the generalised human peripheral sensory nerve fibre model, based on a combination of the models by Rattay et al. (2001) and Blight (1985) and constructed using human sensory nerve fibre morphometric data. However, Bostock et al. (1997) included a persistent sodium current in addition to a transient sodium current, and was therefore able to better explain chronaxie times compared to a model that only included the transient sodium current. Therefore the sensory nerve fibre model described in this article included this additional persistent sodium current.

The objective of this article is to determine if the human Ranvier node model, which is based on a modified version of the HH model can predict the excitability behaviour in human peripheral sensory nerve fibres with diameters ranging from 5.0 – 15.0 μm. The Ranvier node

model is extended to include a persistent sodium current and is incorporated into a single cable nerve fibre model. Parameter temperature dependence is included.

Methods

1. Parameters applied to the nerve fibre model

Rattay et al. (2001) developed a nerve fibre cable model which assumes a propagating action potential driven by Hodgkin-Huxley (Hodgkin and Huxley 1952) dynamics. The model consists of dendritic, somal and axonal sections. The dendritic and axonal sections are divided into cylindrical compartments, with alternative compartments representing unmyelinated Ranvier nodes and myelinated internodes. Membrane potential (V_n) change at the centre of the n^{th} compartment is described by the cable equation

$$C_{m,n}\frac{d\left(V_n\right)}{dt}=\left[-I_{ion,n}+\frac{\left(V_{n-1}+V_{e,n-1}\right)-\left(V_n+V_{e,n}\right)}{R_{n-1}/2+R_n/2}+\frac{\left(V_{n+1}+V_{e,n+1}\right)-\left(V_n+V_{e,n}\right)}{R_{n+1}/2+R_n/2}\right] \quad (1)$$

with the membrane potential given by $V_n = V_{i,n} - V_{e,n} - V_{res}$, offset by the resting membrane potential (V_{res}) and having an initial value $V_n(0)$ equal to zero. $C_{m,n}$ is the membrane capacitance and R_n the axoplasmic resistance to the neighbouring sections at the n^{th} compartment.

The proposed human nerve fibre model was based on the Rattay model, but consisted of an axonal section only (Fig. 1). Parameter values describing the ionic and leakage conductances,

corresponding equilibrium potentials, resting membrane potential and membrane capacitance of the original HH model were modified to reflect the corresponding parameter values for human, with the equations left unaltered. The modelled nerve fibre was externally stimulated with a monopolar electrode positioned sufficiently far away so that the propagating action potential was minimally distorted by the external potential field (V_e). The Ranvier nodes were considered unmyelinated active axolemmae utilising the new human Ranvier node model dynamics described by Smit (2008) and Smit et al. (2009). For completeness, the human nodal model equations will be given here, together with model parameter values (Tables 1 and 2), but for a more comprehensive description please refer to Smit et al. (2009).

---------- *Suggested position of Figure 1* ----------

In myelinated nerve fibres the total nodal sodium current (I_{Na}) is subdivided into two functionally distinct currents. The transient (I_{Nat}) current constitutes the largest proportion (~98%) and has fast activating and inactivating kinetics. The smaller current (~2%) activates equally fast, but at membrane potentials 10 – 20 mV more negative than the transient, and inactivates slowly or not at all; thus forming a persistent (I_{Nap}) current (Burke et al. 2001). Schwarz et al. (1995) developed a human Ranvier node model including only I_{Nat}. Bostock and Rothwell (1997) developed a similar model to the one by Schwarz et al. (1995) and estimated chronaxie times of 176 μs at skin temperature. When they changed their model to include a 2.5% I_{Nap} activated at 10 – 20 mV more negative than I_{Nat} and the sodium activation slowed by a factor 2, the chronaxie time increased to 535 μs. The present human nerve fibre model therefore included a 2.5% I_{Nap} in addition to a 97.5% I_{Nat}. The persistent current was set to activate at 20 mV more negative than the transient current and the sodium activation was slowed down.

The ionic membrane currents in the present human nerve fibre model could therefore be described in terms of temperature-dependent sodium (g_{Na}), potassium (g_K) and leakage (g_L) ionic conductances[2], as well as ionic equilibrium potentials

$$I_{ion}(T) = g_K^{\max}(T) n^4 \left(V - V_K(T)\right) + 0.975 g_{Na}^{\max}(T) m_t^{\,3} h \left(V - V_{Na}(T)\right) + 0.025 g_{Na}^{\max}(T) m_p^{\,3} h \left(V - V_{Na}(T)\right) + g_L(T)\left(V - V_L(T)\right) \quad \left[\mu A / cm^2\right]. \tag{2}$$

Ionic currents are considered ohmic and are given in terms of the ionic conductances and change in membrane potential. Ion channel activation and inactivation probability dynamics (m_t, m_p, h and n respectively) were described by

$$\frac{dx}{dt} = \alpha_x(V)\left[1 - x\right] - \beta_x(V)\, x, \;\; x = m_t, m_p, n, h \tag{3}$$

with initial values $m_t(0) = m_p(0) = 0.05$, $h(0) = 0.6$, $n(0) = 0.32$, and given in terms of the voltage-dependent opening and closing rates of the ion channels $\alpha_x(V)$ and $\beta_x(V)$

$$\alpha_{mt}, \alpha_{ns} = A Q_{10}^{(T - T_0)/10} \cdot \frac{B - CV}{D\left(\exp\left(B - CV\right)\right) - 1} \qquad \left[m/s\right], \tag{4a}$$

$$\beta_{mt}, \beta_{ns}, \alpha_h = A Q_{10}^{(T - T_0)/10} \cdot B \exp\left(\frac{-V}{C}\right) \qquad \left[m/s\right], \tag{4b}$$

[2] Conductances in the paper are the maximum conductances for the specific ion species, with the superscript 'max' indicated in eq. (2) but omitted in the text referrals.

$$\beta_h = AQ_{10}^{(T-T_0)/10} \cdot \frac{1}{1+\exp\left(B-CV\right)}, \qquad \left[m/s\right] \tag{4c}$$

$$\alpha_{mp} = AQ_{10}^{(T-T_0)/10} \cdot \frac{B-C\left(V-\Delta V\right)}{D\left(\exp\left(B-C\left(V-\Delta V\right)\right)\right)-1} \qquad \left[m/s\right], \tag{4d}$$

$$\beta_{mp} = AQ_{10}^{(T-T_0)/10} \cdot B\exp\left(\frac{-\left(V-\Delta V\right)}{C}\right) \qquad \left[m/s\right], \tag{4e}$$

where ΔV indicates that the persistent sodium current activated 20 mV more negative than the transient sodium current. Acceleration of the activation and inactivation of the membrane's permeability to specific ion species, as suggested by Huxley (1959), are given by parameter *A* values (Table 1). In accordance with Bostock and Rothwell (1997), activation of the sodium permeability of I_{Nap} was slowed down by a factor 2.2. Parameters *B*, *C* and *D* are the parameter values from the original HH model (Hodgkin and Huxley 1952) equations as used by Rattay et al. (2001), and are considered constant.

---------- *Suggested position of Table 1.* ----------

The equilibrium potentials were given in terms of the Nernst potential equations for the different ion species (Hille 2001)

$$V_{Na}, V_K, V_L = \frac{1000RT_K}{F}\ln\left(\frac{\left[ion\right]_o}{\left[ion\right]_i}\right) - V_{rest} \quad \left[mV\right] \tag{5}$$

with R the universal gas constant, F the Faraday constant, T_K the absolute temperature (in Kelvin) and $[ion]_o/[ion]_i$ the extracellular to intracellular ion concentration ratio for Na^+, K^+ and leakage ions respectively (Table 2).

---------- *Suggested position of Table 2.* ----------

In an additional modification to the original Rattay cable model the myelinated internodes were considered to be single cable structures as modelled by Blight (1985). The leaky myelin sheath and axolemma were combined together in series, having a high resistance and low capacitance. The internodal capacitance (c_{int}) was given by

$$c_{\text{int}} = \left(\frac{1}{c_{mem}} + \frac{N_{my}}{c_{my}} \right)^{-1} \quad \left[\mu F / cm^2 \right], \tag{6}$$

with c_{mem} the same value as the nodal membrane capacitance and c_{my} the myelin membrane capacitance (Table 2). The number of myelin layers (N_{my}) was given by

$$N_{my} = \left\lfloor 0.5\left(d_f - d_a \right) \right\rfloor / l_{my}, \tag{7}$$

with d_f the total internodal nerve fibre diameter (cm), d_a the internodal axolemmal diameter (cm) and l_{my} the myelin layer thickness equal to 0.016 μm (Blight 1985).

The internodal conductance (g_{int}) was given by

$$g_{\text{int}}(T) = \frac{1}{\left(N_{my} R_{my}(T)\right) + R_{mem}(T)} \quad \left[mS/cm^2\right], \tag{8}$$

with R_{my} the temperature-dependent myelin membrane resistance and R_{mem} the temperature-dependent axolemmal membrane resistance (Table 2 and Blight (1985)).

The ionic membrane currents under the myelin sheath are ignored and this leads to the assumption of a constant internodal membrane conductance (g_{int}) (Rattay et al. 2001). I_{int} was therefore given by

$$I_{\text{int}}(T) = g_{\text{int}}(T)V \qquad \left[\mu A/cm^2\right]. \tag{9}$$

Similar to Wesselink et al. (1999) the electrical parameters of the nerve fibre cable model were recalculated as values per unit area and optimised for a fibre diameter of 15.0 μm. Electrical parameter values are listed in Table 2. The membrane capacitance ($C_{m,n}$) and axoplasmic resistance (R_n) of the n^{th} compartment are defined in eq. 1. R_n is a function of the axoplasmic resistivity (ρ_{ax}) and the AP's conduction velocity (v_c) is influenced by ρ_{ax} (Moore et al. 1978; Frijns et al. 1994). Human peripheral sensory nerve fibres can be classified into groups according to conduction velocity and fibre diameter (Schalow et al. 1995). Schalow et al. (1995) determined v_c values of about 64.0 m/s for fibres having a diameter of 15.0 μm and about 10.0 m/s for 3.0 – 4.0 μm diameter fibres around 37°C. Frijns et al. (1994) argued that although ρ_{ax} had not been reliably measured before, their model studies suggest a value of 0.07 kΩ.cm at 37°C and a Q_{10} factor of $(1.3)^{-1}$. For the new human nerve fibre cable model a

value of 0.025 kΩ.cm at 37°C for ρ_{ax} and a corresponding Q_{10} factor of $(1.35)^{-1}$ were selected to give a v_c of 58.3 m/s at 37°C for the 15.0 μm diameter axonal fibre.

Wesselink et al. (1999) assumed a fibre diameter of 15.0 μm and a nodal area of 50 μm^2. This results in a nodal length of 1.061 μm, which falls well within the range of 0.88 – 1.25 μm for different nerve fibres (Chiu et al. 1999; Vabnick et al. 1999; Caldwell et al. 2000; Waxman 2000; Scherer and Arroyo 2002). SEM photographs from these studies, as well as morphometric studies on human sensory nerve fibres (Behse 1990), indicate that for internodes the axonal to fibre diameter ratio (g-ratio) varies from 0.57 to 0.7. On average smaller g-ratios are associated with thinner fibres. It appeared that for fibres thicker than 0.34 μm the internodal axolemmal diameter (d_a) varied linearly with the fibre diameter (d_f)

$$d_a = 0.63 d_f - 3.4\times10^{-5} \qquad [cm]. \tag{10}$$

The relationship between d_f and the internodal length (L_{int})

$$L_{\text{int}} = 7.9\times10^{-2} \ln\left(d_f / 3.4\times10^{-4}\right) \qquad [cm], \tag{11}$$

however, was only valid for fibre diameters larger than 3.4 μm (Wesselink et al. 1999). Also apparent from the same SEM photographs is the strangulation of the Ranvier node (Chiu et al. 1999; Vabnick et al. 1999; Caldwell et al. 2000; Waxman 2000; Scherer and Arroyo 2002). Nodal diameter data from these SEM photographs were plotted against their corresponding d_f values, which ranged from 6.29 μm to 12.0 μm, and a curve fitted through

the data points in Matlab. The best fit for the nodal diameter (d_{node}) was a third order polynomial

$$d_{node} = 8.502\times10^{5}\left(d_f\right)^3 - 1.376\times10^{3}\left(d_f\right)^2 + 8.202\times10^{-1}d_f - 3.622\times10^{-5} \quad [cm], \quad (12)$$

and this was confirmed by the fitting the curve in Sigmaplot using a different fitting procedure. Assuming a Ranvier node of cylindrical shape (Rattay 1990) and having a constant nodal length of 1.061 μm irrespective of fibre diameter (refer to Fig. 1), this resulted in nodal diameters smaller than the 50 μm^2 employed by Wesselink et al. (Wesselink et al. 1999).

2. Model output calculations

All calculations were performed in Matlab. Differential equations were too stiff to be solved using the ode45 and ode23t numerical solvers, and hence the ode15s solver was used[3]. Modelled nerve fibres ranged from 5.0 – 15.0 μm in diameter and were externally stimulated using a monopolar external electrode placed 1.0 cm from the nerve fibre central axis. The external environment was considered infinite, isotropic and homogeneous with an external resistivity (ρ_e) of 0.3 kΩ.cm at 37°C (Frijns et al. 1994). External stimulation was thus considered purely resistive and given by

[3] The ode15s solver is a multistep solver with variable timestep. It is a built-in Matlab function based on the numerical differentiation formulas (NDFs), or optionally the backward differentiation formulas (BDFs, also known as Gear's method) (From the Matlab Help files).

$$V_e = \frac{\rho_e I_{stim}}{4\pi r_{dist}} \qquad [mV] \tag{13}$$

with r_{dist} the distance between the node and the electrode.

Action potential (AP) characteristics include amplitude, rise and fall times, strength-duration behaviour, refractory period and conduction velocity. Rise and fall times were calculated by approximating the AP by a triangle, with the apex at the maximum amplitude (Frijns and ten Kate 1994). The rising edge intersects the action potential curve at 10% of the maximum amplitude and the rise time is calculated as the time difference between this intersection point and the apex. The falling time is calculated in the same manner using the falling edge.

Strength-duration behaviour is characterised by the rheobase current and chronaxie time. Stimulation pulses were monophasic-anodic and ranged from 0.2 – 2.0 ms in duration. Even though the external stimulation was considered purely resistive, at temperatures lower than 30°C the strength-duration curves for stimulation pulses up to 1.0 ms could not be fitted with the Weiss linear relationship (Weiss 1901; Bostock 1983; Wesselink et al. 1999). Strength-duration curves were thus fitted with the exponential relationship of Lapicque (1907)

$$I_{th} = I_{rb} \Big/ \left(1 - e^{(-t/\tau_{sd})}\right) \tag{14}$$

with I_{th} the threshold current (μA), t the pulse duration (μs), I_{rb} the rheobase current (μA) and τ_{sd} the strength-duration time constant (μs). The chronaxie time (τ_{ch}) is the strength-duration time constant at twice I_{rb}.

Absolute (ARP) and relative (RRP) refractory periods characterise nerve fibre refractory behaviour. Initial nerve fibre stimulation was effected with a 0.1 ms monophasic pulse with amplitude 20% above I_{th}. Stimulation with a second 0.1 ms monophasic pulse had to result in a second propagating AP to calculate refractory periods. The absolute refractory period was defined as the maximum interval between the two pulses in which no second pulse, with amplitude of up to 400% I_{th}, could be elicited. The relative refractory period was the minimum interval between the two pulses in which a pulse of at most 101% I_{th} was required to elicit the second AP (Wesselink et al. 1999).

Results

A general human peripheral sensory nerve fibre having diameters in the range of 5.0 – 15.0 μm was simulated in Matlab and externally stimulated with a monopolar electrode. Stimulation pulses were square, monophasic-anodic and only single pulses were used.

1. Action potential rise and fall times

AP rise and fall times were calculated in the temperature range of 20 – 37°C. Fig. 2 shows an example of a propagating AP for a 15.0 μm fibre calculated at 20°C. Rise and fall times for a 15.0 μm fibre are compared to experimentally estimated results (Table 3). Rise times were less than 0.5% shorter than the experimental results at both 20 and 25°C, while being 4.2% shorter at 37°C. The rise time decreased by 24.5% (Q_{10} factor of $(1.76)^{-1}$) from 20 to 25°C.

---------- *Suggested position of Figure 2* ----------

---------- *Suggested position of Table 3* ----------

Fall times were 6% longer at 20°C and 2.7% shorter at 25°C than the experimental results, while being 60% longer at 37°C. Similar to the results of the Ranvier node model (Smit et al. 2009) the fall time decreased by 22.6% (Q_{10} factor of $(1.66)^{-1}$) from 20 to 25°C. This decrease was steeper than the 20% decrease observed for the experimental results.

Calculated rise and fall times, and hence AP duration, varied with fibre diameter (Fig. 3). In general, independent of temperature, rise times increased with a decrease in fibre diameter down to 7.5 μm (Fig. 3a). However, below 7.5 μm rise times decreased again, with the rise time of a 5.0 μm diameter fibre similar to the rise time of a 12.5 μm diameter fibre.

---------- *Suggested position of Figure 3* ----------

Fall times decreased between 15.0 μm and 10.0 μm and then increased again for smaller fibre diameters, with the fall time of a 5.0 μm diameter fibre being similar to the fall time of a 15.0 μm diameter fibre (Fig. 3b). The relationships between rise or fall times and fibre diameter became more pronounced as the temperature was decreased from body temperature. So, for example, the slopes of the fall time curve at 25°C were more than twice as steep as the corresponding curve slopes at 37°C (Fig. 3b).

The relative sensitivity of the rise and fall times on the Ranvier node model parameters was discussed in Smit et al. (2009). In this study the cable model by Rattay et al. (2001) was extended to include temperature dependence of the axoplasmic resistivity (ρ_{ax}) and the fibre

dependence of the axonal diameter (d_a) and nodal diameter (d_{node}). Even though the internodal length is also dependent on the fibre diameter, the relationship used by Wesselink et al. (1999) was assumed correct and its influence on the nerve fibre's characteristics will not be discussed here.

Figs. 4a and b show the influence of the persistant sodium (I_{Nap}) current and the nodal and axonal diameters on the rise and fall times of an AP calculated at 25°C. The addition of the I_{Nap} current did not influence the AP rise time, but increased the fall time by about 1.1% when compared to a nerve fibre model containing only a transient sodium (I_{Nat}) current.

The axonal and nodal diameters were varied respectively by changing the parameter values, while keeping all other parameters constant for the model containing both I_{Nap} and I_{Nat} currents. A larger axonal diameter was effected by replacing eq. 10 with the relation

$$d_a = 0.8 d_f - 1.8 \times 10^{-4} \qquad [cm],$$

utilised by Wesselink et al. (1999). Use of the larger axonal diameter lead to an increase in the rise times of fibre diameters larger than 7.5 μm and shorter fall times over all fibre diameters, but in general rise and fall times followed the trends as for the smaller axonal diameter.

In contrast, rise times changed less than 6.3% and fall times less than 1.4% over the fibre diameter range when the nodal diameters were kept equal to the axonal diameters, i.e. nodal strangulation was ignored. Wesselink et al. (1999) did not implement nodal strangulation, but opt for a model where the nodal diameter equalled the axonal diameter. They observed that

the AP rise and fall times did not change significantly with a change in fibre diameter. The results obtained here therefore compared well to their observation.

The most commonly used value for ρ_{ax} is 0.07 kΩ.cm at 37°C and a Q_{10} factor of $(1.3)^{-1}$ (see for example Frijns et al. 1994). Wesselink et al. (1999) used a value of 0.033 kΩ.cm at 37°C without any temperature dependence. Our model suggested a value of 0.025 kΩ.cm at 37°C and a corresponding Q_{10} factor of $(1.35)^{-1}$. The influence of ρ_{ax} on the AP rise and fall times calculated at 25°C was investigated using these three different values and two corresponding Q_{10} factors (Figs. 4c and d). An increase in the ρ_{ax} value resulted in a skewing of the AP shape, with an increase in rise times of at most 10.0% and a decrease in fall times of at most 6.3%, irrespective of Q_{10} value.

2. Action potential duration times

The AP duration is the sum of the rise and fall times and displays an inverse relationship to the fibre diameter (Paintal 1966). At temperatures higher than 27°C, AP duration followed this inverse relationship trend for all fibre diameters larger than 7.5 μm (Fig. 5), but not so for fibre diameters smaller than 7.5 μm. At lower temperatures this relationship did not hold for fibre diameters larger than or equal to 12.5 μm.

---------- *Suggested position of Figure 5* ----------

---------- *Suggested position of Figure 6* ----------

Normalisation of the AP duration curves (for different fibre diameters) to their respective values at 37°C indicated a slightly steeper increase in AP duration in the thicker fibres compared to the thinner fibres when the temperature was decreased; the average Q_{10} factor being about $(1.65)^{-1}$ (Fig. 6). The curve of the 5.0 μm diameter fibre was similar to the 12.5 μm diameter curve and was thus omitted from the figure.

---------- *Suggested position of Figure 7* ----------

Not apparent from Fig. 6 is the change in slope around 27°C for all fibre thicknesses. For fibres thicker than 7.5 μm, the slopes increased by about 5.6% in the temperature range above 27°C, compared to the less steep slope of about 3% in the temperature range below 27°C (Fig. 7).

3. Action potential amplitude

Calculated amplitudes followed the trend of an amplitude decrease with temperature increase (Buchthal and Rosenfalck 1966; Schwarz and Eikhof 1987; Frijns et al. 1994; Wesselink et al. 1999). For the 15.0 μm fibre amplitudes around 115 mV were obtained at 20 and 25°C and decreased by less than 1% between 20 and 25°C. At 37°C an amplitude around 112 mV was obtained. This trend in amplitude decrease with a decrease in temperature was true for all fibres thicker than 5.0 μm, with amplitude values being larger than 100 mV. The exception to this trend again was the 5.0 μm fibre with amplitudes comparable to those of the 12.5 μm fibre.

4. Conduction velocities

Conduction velocity (v_c) values of the new human nerve fibre cable model exhibited fibre diameter dependency (Fig. 8), as well as temperature dependency (Table 4).

---------- *Suggested position of Figure 8* ----------

---------- *Suggested position of Table 4* ----------

For fibre diameters thicker than 12.5 μm, v_c values compared well with the values measured by Schalow et al. (1995), but for thinner fibres v_c values were underestimated. Values were undervalued for all fibre diameters thicker than 5.0 μm compared to values estimated by Wesselink et al. (1999). Conduction velocities per diameter varied from 2.9 – 3.5 μs^{-1} for fibre diameters ranging from 5.0 – 15.0 μm at 37°C. Lowitzsch et al. (1977) measured average v_c values for human ulnar nerve sensory nerve fibres. Comparison to the data of Schalow et al. (1995) suggests an average ulnar fibre diameter of about 13.0 μm. Hence the v_c temperature dependency of a 13.0 μm simulated nerve fibre is compared to the results achieved by Lowitzsch et al. (1977) (Table 4). Simulated v_c values decreased with increased temperature, but at a slower rate compared to real nerve fibre data. The maximum simulated value of 46.20 $m.s^{-1}$ at 35°C was 6.2% lower than the experimentally measured value. Similar to the experimental results, the Q_{10} factors were different for the temperature ranges 20 – 30°C (Q_{10} factor of 1.47) and 25 – 35°C (Q_{10} factor of 1.27).

---------- *Suggested position of Figure 9* ----------

The biggest influence on v_c was due to the axoplasmic resistivity (ρ_{ax}) (Fig. 9). Larger values of ρ_{ax} lead to a decrease in v_c values, irrespective whether a Q_{10} factor of $(1.3)^{-1}$ or $(1.35)^{-1}$ was chosen. This decrease was more pronounced in thicker fibres than thinner fibres. Changes in the fibre dependence of the axonal diameter (d_a) and nodal diameter (d_{node}) resulted in v_c values less than 7.0% lower compared to values for the generalised sensory nerve fibre cable model as calculated at 37°C.

5. Refractory periods

ARP and RRP of the 13.0 μm simulated nerve fibre is compared to the results (Table 4) obtained by Lowitzsch et al. (1977). At body temperature (37°C) the ARP was 0.9 ms and the RRP 3.05 ms. Both ARP and RRP decreased with an increase in temperature. Q_{10} factors indicated that the decrease was more pronounced in the lower temperature range of 20 – 30°C than in the higher range of 25 – 35°C, similar to the trend observed experimentally. For RRP the calculated rates overestimated the experimentally estimated rates by less than 15.0%. However, for ARP the calculated results underestimated the experimental rates by more than 40%. Simulated ARP values did not vary significantly for fibres thicker than 10.0 μm, but increased by about 30% when the fibre diameter was decreased to 5.0 μm.

6. Strength-duration relationships

Strength-duration curves were calculated for nerve fibres in the range of 5.0 – 15.0 μm. Stimulation was performed with a single monopolar external electrode placed 1.0 cm from the nerve fibre central axis. Stimulation pulses were monophasic-anodic and ranged from

0.2 – 2.0 ms in duration. The chronaxie time constant (τ_{cd}) showed nerve fibre diameter dependence (Fig. 10), ranging from 128.5 μs to 183.0 μs at 37°C over the studied nerve fibre diameter range. However, unlike the results obtained by Wesselink et al. (1999), τ_{cd} values did not decrease monotonically with an increase in fibre diameter, but increased again for fibre diameters larger than 10.0 μm. Strength-duration times (τ_{sh}) were about 30.5% higher than τ_{cd} values for all fibre diameters. Rheobase current was increased by 51.0% by increasing the fibre diameter from 5.0 μm to 10.0 μm and decreased by 11.6% for a further diameter increase to 15.0 μm.

The increase in τ_{cd} values was even more pronounced for a nerve fibre containing only an I_{Nat} current. However, when nodal strangulation in the model containing both I_{Nat} and I_{Nap} currents was ignored, τ_{cd} values followed the trend of the Wesselink et al. (1999) results, with values ranging from 146.1 μs to 219.6 μs.

---------- *Suggested position of Figure 10* ----------

---------- *Suggested position of Figure 11* ----------

Strength-duration relationships were calculated at temperatures between 20 and 37°C with τ_{ch} values showing an inverse relation to temperature, ranging from 138.4 – 737.4 μs (Fig. 11). This relationship was non-linear, with a larger rate of increase in τ_{ch} values for the temperature range 20 – 30°C (Q_{10} factor of $(3.01)^{-1}$) compared to the range 25 – 37°C (Q_{10} factor of $(2.62)^{-1}$), as calculated for a fibre of diameter 12.5 μm. The same trend was evident for the other fibre diameters as well. For the nerve fibre containing only an I_{Nat} current, τ_{ch} values also followed a non-linear relationship with values ranging from 145.9 – 605.3 μs. The

non-linear relationship, however, was less pronounced than for the nerve fibre containing both I_{Nat} and I_{Nap} currents. By excluding the effect of nodal strangulation, the rate of increase was lessened to factor 3.2, compared to a factor 5.3 when nodal strangulation was included. The rate of increase relationship, however, was still non-linear.

Discussion

In this study a new generalised human peripheral sensory nerve fibre cable model was developed. The nerve fibre model was based on the cable model by Rattay et al. (2001), but modified to a cable structure based on the model of Blight (1985). Modelled Ranvier nodes utilised the human Ranvier node model dynamics by Smit (2009), together with the added persistent sodium (I_{Nap}) current. The temperature dependence of all parameters was included.

Single-cable nerve fibre models do include a small fast potassium (I_{Kf}) current, but since the myelin is considered a near perfect insulator with high resistance, the modelled nodes have to set their own resting potential (see for example the human nerve fibre models by Schwarz et al. 1995; and Wesselink et al. 1999). This is effected through the inclusion of a high conductance leakage current (I_L), mostly carried by K^+ (Baker 2002). In the present human nerve fibre model the extracellular to intracellular ion concentration ratios for the I_L and I_K currents were similar, suggesting that I_L was mostly carried by K^+ (see the discussion in Smit et al. 2009). However, in this model the myelin was not considered a near perfect insulator, resulting in smaller g_L values than the values used in the existing human nerve fibre models.

AP rise and fall times showed fibre diameter dependence (Fig. 3) as well as temperature dependence (Table 3). The influence of temperature dependence of the axoplasmic resistivity

(ρ_{ax}), the fibre dependence of the axonal diameter, as well as a model containing only a transient sodium (I_{Nat}) current on the rise and fall times for different fibre diameters indicated the conservation of the same trends observed for the human sensory nerve fibre, albeit at slightly different values (Figs. 4a to d). The greatest influence was obtained when nodal strangulation was ignored (Figs. 4a and b), i.e. the nodal diameter was equated to the axonal diameter. Rise and fall times showed an almost complete fibre independence, similar to the Wesselink et al. (1999) model. It therefore seems that the non-monotonic behaviour over fibre diameter dependence could be attributed to the inclusion of the relationship describing the nodal strangulation. This relationship has not been mathematically described or implemented in previous models. There also exist a scarcity and incompleteness of experimental data regarding the rise and fall times of fibres having different calibres. The equation implemented in the present model was a first attempt at inclusion of this parameter and it can be concluded that a more realistic description will only be possible once such experimental data have become available.

Temperature dependence of rise times were well predicted compared to experimental results, but the predicted fall time at 37°C was 60% longer than the value predicted by the Wesselink et al. (1999) model for a 15.0 μm diameter nerve fibre. The temperature influence of the individual parameters of the Ranvier node model on the AP rise and fall times was discussed in Smit et al. (2009). Rise and fall times depended significantly on the sodium activation and inactivation kinetics respectively and the fall times less than 1% on the potassium kinetics (Smit et al. 2009). The optimised sodium inactivation Q_{10} factor of 1.5 was very close to the estimated value of 1.56 observed by Schwarz et al. (1995) for the decrease in fall time between 20 and 25°C, but was about a factor two less than the value of 2.9 used in previously developed models (Schwarz and Eikhof 1987; Schwarz et al. 1995; Wesselink et al. 1999).

Considering the influence of the nodal diameter on the rise and fall times, it is to be expected that rise and fall times of thinner fibres will have similar values than the 15.0 μm diameter nerve fibre when nodal strangulation is ignored.

Paintal (1966) demonstrated an inverse relationship between AP duration and conduction velocity in cat sensory nerve fibres. AP duration also varies inversely with temperature in both slow and fast conducting fibres, although the slopes of these curves change at 27°C. In slow conduction fibres the slopes are almost the same for the temperature ranges below and above 27°C respectively, having Q_{10} factors around $(3.1)^{-1}$ below 27°C and $(3.4)^{-1}$ above 27°C (refer to Fig. 4 in Paintal 1966). The slopes for fast and slow conducting fibres are almost the same for temperatures above 27°C. However, for temperatures below 27°C, the slopes become levelled off in the faster fibres, having a Q_{10} factor of about $(2.27)^{-1}$ for a 64 $m.s^{-1}$ fibre. This constitutes a 26.7% decrease in slope between slow and fast fibres.

In the human sensory nerve fibre model the inverse relationship between AP duration and fibre thickness, i.e. conduction velocity, held for simulated fibres thicker than 7.5 μm. AP duration varied inversely with temperature, but with the average Q_{10} factor for the slopes only being only about $(1.65)^{-1}$, compared to the value of $(3.4)^{-1}$ for the results obtained by Paintal (1966). Similar to the results of Paintal (1966), the curve slopes changed around 27°C, but became steeper instead of flatter (see Fig. 7). However, when the increase in slope steepness with increased fibre thickness for the temperature range below 27°C was compared with the slope steepness increase for the temperature range above 27°C, the former increased by about 3.0% compared to the 5.3% of the latter. In the thicker fibres the overall slope also changed less than 1% between the two temperature ranges, compared to a change of about 1.8% in the thinner fibres. It therefore seemed that the modelled human nerve fibres displayed the same

trend of levelled off slopes in thicker (i.e. faster) fibres for temperatures below 27°C, albeit a factor 10 less than for fibres in the Paintal (1966) study.

Schalow et al. (1995) determined that the ratio of the conduction velocity (v_c) to fibre diameter in afferent sensory nerve fibres ranges between 2.5 μs^{-1} and 4.1 μs^{-1}. In the model by Wesselink et al. (1999), the ratio varies between 3.1 μs^{-1} and 4.3 μs^{-1} for fibre diameters in the range of 5.0 – 15.0 μm at 37°C. In the present human sensory nerve fibre model the simulated conduction velocity to fibre diameter ratios of 2.9 – 3.5 μs^{-1} compared well with previous results. However, v_c values were underestimated compared to the results of Schalow et al. (1995) and Wesselink et al. (1999) and did not display the linear relation to fibre diameter as the results of Wesselink et al. (1999) did. An analysis of the sensitivity of the v_c to model parameters suggested that v_c values were most sensitive to the internodal length and, to a lesser degree, the axoplasmic resistivity (ρ_{ax}) (Fig. 9). For the present human nerve fibre cable model the values for ρ_{ax} and its corresponding Q_{10} factor were selected to give a v_c of 58.3 m/s at 37°C for the 15.0 μm diameter axonal fibre. However, the same analysis study suggested different ρ_{ax} values when the internodal length for the 15.0 μm diameter fibre was varied. This added an additional degree of freedom to the optimisation procedure and would have required optimisation not only for a 15.0 μm diameter fibre, but also for fibres of different diameters. Owing to the lack of sufficient parameter data for fibres other than the 15.0 μm diameter fibre, it was assumed that it would be feasible to use the same relationship between fibre diameter and internodal length as Wesselink et al. (1999). This resulted in the new model having the same internodal lengths as the model of Wesselink et al. (1999), but with a smaller ρ_{ax} value.

Most mammalian nerve fibre models use a value of 0.07 kΩ.cm for ρ_{ax} at 37°C and a Q_{10} factor of $(1.3)^{-1}$ (see for example Halter and Clark Jr 1991; and Frijns et al. 1994), although Frijns et al. (1994) did mention that ρ_{ax} had not been reliably measured before. The Rattay et al. (2001) cable model used a constant value of 0.05, independent of temperature. The Wesselink et al. (1999) model was based on the experimental work and model by Schwarz et al. (1995). The latter study did not report any ρ_{ax} values and hence Wesselink et al. (1999) optimised the ρ_{ax} value to simulate v_c values similar to experimental v_c values from, among others, Schalow et al. (1995). They hence used a value of 0.033 kΩ.cm at 37°C without any temperature dependence. The present study employed the same strategy as Wesselink et al. (1999), but was not able to reach such accurate predictions of v_c values without using a too low ρ_{ax} value. This difference in value compared to other human nerve fibre cable models might account for the underestimated simulated v_c values. The implementation of a double cable model might be required to predict a more realistic ρ_{ax} value, and could be the topic of a follow-up study.

The calculated ARP of about 0.9 ms at 37°C was longer than the experimentally estimated range of 0.58 – 0.79 ms for humans (refer to Table 1 in Wesselink et al. 1999). The relation between APR and fibre diameter was similar to the findings of Paintal (1965), who found that in cat nerve fibres, ARP values in faster (i.e. thicker) fibres varied insignificantly, but they varied inversely to v_c in slower fibres. Calculated RRP of 3.05 ms compared favourably with experimental results of about 3.0 ms at 37°C (Lowitzsch et al. 1977; Wesselink et al. 1999). ARP times depend on the AP rise and fall times (White 2002). Overestimation of the AP's fall time of almost a factor two (Table 3) resulted in an overestimation of ARP values at 37°C. This overestimation increased for thinner fibres and correlated with the increase in AP duration for thinner fibres (refer to Figs. 3 and 5). Similar arguments hold for explanations of

the ARP values at lower temperatures. As discussed earlier in this section, re-optimisation of the sodium inactivation kinetics may therefore be required to improve predicted AP fall times, resulting in more realistic ARP values.

Strength-duration behaviour indicated fibre diameter dependency, but unlike the model of Wesselink et al. (1999), rheobase current, strength-duration time constants and hence also chronaxie times did not decrease monotonically with a fibre diameter increase. Chronaxie times where shorter than experimentally estimated times (refer to Table 1 in Wesselink et al. 1999). It must be remembered, however, that the experimental values were estimated from compound fibre data (see for example studies by Burke et al. 1999; and Kiernan et al. 2001), in contrast to the single fibre data presented here. Even so the chronaxie times compared favourably with times ranging from 113 – 202 μs from the Wesselink et al. (1999) model. Different experimental studies on the effect of temperature on the chronaxie times in human cutaneous afferent nerve fibres show that chronaxie times do not vary significantly with a change in temperature (Mogyoros et al. 1996; Burke et al. 1999; Kiernan et al. 2001). Simulated results from the present human nerve fibre model were in contrast to these findings, showing an increase of more than a factor 5 for a decrease in temperature from 37°C to 20°C (see Fig. 11). For the nerve fibre containing only the I_{Nat} current, the increase was about a factor four over the same temperature range. When nodal strangulation was ignored the increase dropped to a factor three. This difference in strength-duration behaviour with temperature was not observed in previous human nerve fibre studies (compare Wesselink et al. 1999). The inclusion of the nodal strangulation significantly influenced the trend followed by chronaxie times for both fibre diameter and temperature dependence (Figs. 10 and 11). Given the close link between refractive period values and chronaxie times (White

2002), however, the deviation of the ARP values from experimental data might attribute to the non-monotonic behaviour of the predicted chronaxie times.

Bostock (1983) suggested that the linear relationship of Weiss (1901) best estimates chronaxie times in simulated myelinated nerve fibres. Mogyoros et al. (1996) confirmed this finding for experimentally estimated chronaxie times in compound fibre data. Strength-duration curves at temperatures below 30°C for single human nerve fibres modelled in the present study could not be fitted with the Weiss relationship, and were hence fitted with the exponential relationship of Lapicque (1907). As the temperature was increased from 20°C, exponential fitting became less accurate; suggesting that a hyperbolic fit might be more accurate.

Parameter data used in the new human sensory nerve fibre model were determined from published data from various studies of human nerve fibres. As mentioned in the Methods section, Frijns et al. (1994) argued that ρ_{ax} had not been reliably measured before. Wesselink et al. (1999) derived their fibre-diameter-to-internodal-length relation from published data by Behse (1990). The third order polynomial relationship between nodal diameter and fibre diameter was determined by curve fitting to data derived from SEM photographs. Even though the size estimation of myelinated peripheral nerve fibres is commonly performed in quantitative neuromorphology, Geuna et al. (2001) cautioned that the different methodologies used in such studies may bias the results. Newer computer-automated measurement approaches are more efficient and have a higher accuracy than older manual methods (Geuna et al. 2001). However, the data that were available to determine the model parameter values did come from older studies and parameter values might be different from the true values for *in vivo* nerve fibres. Since the strength-duration properties of a nerve fibre depend on nodal

membrane properties (Bostock 1983), such differences might account for the discrepancy found in chronaxie values; for both temperature and fibre diameter variations.

Furthermore, the temperature dependency of a large proportion of the parameters was effected through the use of Q_{10} factors, in view of a lack of temperature-dependent studies done on individual human nerve fibre parameters. The use of Q_{10} factors assumed an exponential relation between the parameter values and temperature variation (refer for example to the relevant equation in Wesselink et al. 1999). For Q_{10} values close to 1.0, this resulted in a nearly linear relationship over the temperature range 20 – 37°C. Temperature dependency results from this study suggested the assumption of such almost linear relationships over the entire temperature range from 20 – 37°C might not be valid.

Up to now physiologically and morphometrically correct nerve fibre models describing excitability behaviour in human sensory nerve fibres are based on the Goldman-Hodgkin-Katz (GHK) current and voltage equations (Schwarz et al. 1995; Wesselink et al. 1999). As the HH model equations were derived for an unmyelinated nerve fibre, reservations exist about their applicability to describe action potential propagation in myelinated mammalian nerve fibres adequately. In the HH model the current-voltage relation of open Na^+ and K^+ channels is described by the linear relation of Ohm's law. Hille (2001) discussed that since open Na^+ and K^+ channels in vertebrates have small non-linear instantaneous rectification currents, the permeability parameters P_{Na} and P_K of the GHK current equation will provide better empirical estimates of the opening and closing of the ion channels than the conductances (g_{Na} and g_K) of the HH model. He hence suggested that the linear relations of Ohm's law in the HH model be replaced by the GHK current equation in mammals. The original intent with the present study was to investigate the possibility of modifying the

Rattay et al. (2001) human ANF model to a more comprehensive model that incorporated human peripheral ANF characteristics. As discussed in the Introduction section, such characteristics have not been measured before in humans. An interim model of a generalised human peripheral sensory nerve fibre, based on physiological parameters of other peripheral sensory nerve fibre data in humans, was thus developed. The Rattay model utilises the HH model as the membrane model, with the nodal ion channel kinetics accelerated tenfold. We therefore decided to modify the parameter values describing the ionic and leakage conductances, corresponding equilibrium potentials, resting membrane potential and membrane capacitance of the original HH model to reflect the corresponding parameter values for human, but leave the equations unaltered as did the Rattay model. Hence the suggestion by Hille (2001) mentioned above was not implemented, but could be investigated in a follow-up study.

Lastly, mention must be made of the differences observed in the thinner, especially the 5.0 μm, nerve fibres compared to the thicker nerve fibres. Part of these behaviour differences might be explained by the above-mentioned discussion. However, the membrane parameters of the general nerve fibre were, in accordance with the previous modelling work by Schwarz et al. (1995) and Wesselink et al. (1999), developed and optimised for a 15.0 μm fibre and then 'scaled down' to model thinner fibres. Parameters used in the human Ranvier node model were based on values determined from studies done on thicker sensory nerve fibres (see Smit et al. 2009) and these parameter values may be different in thinner fibres. So for example, the slow potassium current at the Ranvier node is mediated by different KCNQ channels (Taylor et al. 1992; Devaux et al. 2004; Schwarz et al. 2006). Ranvier nodes in thinner fibres showed labelling for KCNQ2 and KCNQ3, while nodes in thicker fibres showed labelling only for KCNQ2 (Schwarz et al. 2006).

Conclusion

The objective of this study was to determine if the recently developed human Ranvier node model, which is based on a modified version of the HH model, could predict the excitability behaviour in human peripheral sensory nerve fibres. Up to now the most physiologically and morphometrically correct nerve fibre models describing these behaviour in humans are based on the Goldman-Hodgkin-Katz (GHK) current and voltage equations (Schwarz et al. 1995; Wesselink et al. 1999). These equations are more complex than the HH model equations used in the present model and are used to replace the linear current-voltage relationships of the opening and closing of the sodium and potassium channels in the HH model with non-linear relationships found in vertebrate excitable cells (Hille 2001). This study was the first to show that the HH model equations could be modified to predict excitability behaviour in humans without using the GHK equations. However, the use of linear relationships to describe the Na^+ and K^+ conductances can be considered a limitation and future development of a more accurate model should include a study on the replacement of these relationships with the non-linear GHK current equation.

Furthermore, temperature dependence of all parameters over the temperature range of 20°C to 37°C was addressed. The human Ranvier node model was incorporated into a cable nerve fibre model and simulation predictions compared favourably with experimentally determined results. However, as in the case of the single human Ranvier node model, chronaxie times were overestimated at temperatures lower than body temperature. This can possibly be attributed to shortcomings in the fitting procedure employed to determine the chronaxie times, the bias in measured parameter values due to the measuring methodologies used, as

well as the possible incorrect assumption of linear parameter relationships to temperature variation, although the deviation of APR values from values measured in real nerve fibres and the inclusion of a relationship describing nodal strangulation had a significant influence on the non-linear behaviour of the chronaxie times. Further study in this regard is advised.

ACKNOWLEDGEMENTS

The authors thank Dr JM Nel and Dr RW Sparrow for helpful discussions on aspects of Physical Chemistry and biological membrane properties, as well as two anonymous reviewers whose comments on an earlier version of the manuscript led to an improved final version. This research has been supported by the National Research Foundation (NRF) of South Africa.

Atkins PW (1995) Physical Chemistry. Oxford University Press, Oxford

Baker MD (2002) Electrophysiology of mammalian Schwann cells. Prog Biophys Mol Biol 78:83-103

Bakondi G, Pór Á, Kovács I, Szucs G, Rusznák Z (2008) Voltage-gated K^+ channel (Kv) subunit expression of the guinea pig spiral ganglion cells studied in a newly developed cochlear free-floating preparation. Brain Res 1210:148-162

Behse F (1990) Morphometric studies on the human sural nerve. Acta Neurol Scand Suppl 82:1-38

Blight AR (1985) Computer simulation of action potentials and afterpotentials in mammalian myelinated axons: The case for a lower resistance myelin sheath. Neuroscience 15:13-31

Bostock H (1983) The strength-duration relationship for excitation of myelinated nerve: Computed dependence on membrane parameters. J Physiol (Lond) 341:59-74

Bostock H, Rothwell JC (1997) Latent addition in motor and sensory fibres of human peripheral nerve. J Physiol (Lond) 498:277-294

Briaire JJ, Frijns JHM (2006) The consequences of neural degeneration regarding optimal cochlear implant position in scala tympani: A model approach. Hear Res 214:17-27

Briaire JJ, Frijns JHM (2005) Unraveling the electrically evoked compound action potential. Hear Res 205:143-156

Bruce IC, White MW, Irlicht LS, O'Leary SJ, Clark GM (1999) The effects of stochastic neural activity in a model predicting intensity perception with cochlear implants: low-rate stimulation. IEEE Trans Biomed Eng 46:1393-1404

Buchthal F, Rosenfalck A (1966) Evoked action potentials and conduction velocity in human sensory nerves. Brain Res 3:1-122

Burke D, Kiernan MC, Bostock H (2001) Excitability of human axons. Clin Neurophysiol 112:1575-1585

Burke D, Mogyoros I, Vagg R, Kiernan MC (1999) Temperature dependence of excitability indices of human cutaneous afferents. Muscle Nerve 22:51-60

Caldwell JH, Schaller KL, Lasher RS, Peles E, Levinson SR (2000) Sodium channel $Na_v1.6$ is localized at nodes of Ranvier, dendrites, and synapses. Proc Natl Acad Sci USA 97:5616-5620

Carlyon RP, van Wieringen A, Deeks JM, Long CJ, Lyzenga J, Wouters J (2005) Effect of interphase-gap on the sensitivity of cochlear implant users to electrical stimulation. Hear Res 205:210-224

Chen WC, Davis RL (2006) Voltage-gated and two-pore-domain potassium channels in murine spiral ganglion neurons. Hear Res 222:89-99

Chiu SY, Ritchie JM, Rogart RB, Stagg D (1979) A quantitative description of membrane currents in rabbit myelinated nerve. J Physiol (Lond) 292:149-166

Chiu SY, Zhou L, Zhang C-L, Messing A (1999) Analysis of potassium channel functions in mammalian axons by gene knockouts. J Neurocytol 28:349-364

Colombo J, Parkins CW (1987) A model of electrical excitation of the mammalian auditory-nerve neruon. Hear Res 31:287-312

Devaux JJ, Kleopa KA, Cooper EC, Scherer SS (2004) KCNQ2 Is a Nodal K+ Channel. J Neurosci 24:1236-1244

Frankenhaeuser B, Huxley AF (1964) The action potential in the myelinated nerve fibre of *Xenopus laevis* as computed on the basis of voltage clamp data. J Physiol (Lond) 171:302-315

Frijns JHM, Mooij J, ten Kate JH (1994) A quantitative approach to modeling mammalian myelinated nerve fibers for electrical prosthesis design. IEEE Trans Biomed Eng 41:556-566

Frijns JHM, ten Kate JH (1994) A model of myelinated nerve fibres for electrical prosthesis design. Med Biol Eng Comput 32:391-398

Geuna S, Tos P, Guglielmone R, Battiston B, Giacobini-Robecchi MG (2001) Methodological issues in size estimation of myelinated nerve fibers in peripheral nerves. Anat Embryol 203:1-10

Glueckert R, Pfaller K, Kinnefors A, Rask-Andersen H, Schrott-Fischer A (2005a) The human spiral ganglion: New insights into ultrastructure, survival rate and implications for cochlear implants. Audiol Neurotol 10:258-273

Glueckert R, Pfaller K, Kinnefors A, Schrott-Fischer A, Rask-Andersen H (2005b) High resolution scanning electron microscopy of the human organ of Corti.: A study using freshly fixed surgical specimens. Hear Res 199:40-56

Grill WM, Mortimer JT (1996) The effect of stimulus pulse duration on selectivity of neural stimulation. IEEE Trans Biomed Eng 43:161-166

Halter JA, Clark Jr JW (1991) A distributed-parameter model of the myelinated nerve fiber. J Theor Biol 148:345-382

Hille B (2001) Ionic Channels of Excitable Membrane. Sinauer Associates Inc., Sunderland, Massachusetts

Hodgkin AL, Huxley AF (1952) A quantitative description of membrane current and its application to conduction and excitation in nerve. J Physiol (Lond) 117:500-544

Hossain WA, Antic SD, Yang Y, Rasband MN, Morest DK (2005) Where is the spike generator of the cochlear nerve? Voltage-gated sodium channels in the mouse cochlea. J Neurosci 25:6857-6868

Huxley AF (1959) Ion movements during nerve activity. Ann N Y Acad Sci 81:221-246

Kiernan MC, Cikurel K, Bostock H (2001) Effects of temperature on the excitability properties of human motor axons. Brain 124:816-825

Lapicque L (1907) Recherches quantitatifs sur l'excitation electrique des nerfs traitee comme un polarisation. J Physiol (Lond) 9:622-635

Lowitzsch K, Hopf HC, Galland J (1977) Changes of sensory conduction velocity and refractory periods with decreasing tissue temperature in man. J Neurol 216:181-188

Macherey O, Carlyon RP, van Wieringen A, Wouters J (2007) A dual-process integrator-resonator model of the electrically stimulated human auditory nerve. J Assoc Res Otolaryngol 8:84-104

Matsuoka AJ, Rubinstein JT, Abbas PJ, Miller CA (2001) The effects of interpulse interval on stochastic properties of electrical stimulation: models and measurements. IEEE Trans Biomed Eng 48:416-424

McIntyre CC, Richardson AG, Grill WM (2002) Modeling the excitability of mammalian nerve fibers: Influence of afterpotentials on the recovery cycle. J Neurophysiol 87:995-1006

Miller CA, Abbas PJ, Rubinstein JT (1999) An empirically based model of the electrically evoked compound action potential. Hear Res 135:1-18

Mo Z-L, Adamson CL, Davis RL (2002) Dendrotoxin-sensitive K^+ currents contribute to accomodation in murine spiral ganglion neurons. J Physiol (Lond) 542:763-778

Mogyoros I, Kiernan MC, Burke D (1996) Strength-duration properties of human peripheral nerve. Brain 119:439-447

Moore JW, Joyner RW, Brill MH, Waxman SD, Najar-Joa M (1978) Simulations of conduction in uniform myelinated fibers. Relative sensitivity to changes in nodal and internodal parameters. Biophys J 21:147-160

Morse RP, Evans EF (2003) The sciatic nerve of the toad Xenopus laevis as a physiological model of the human cochlear nerve. Hear Res 182:97-118

Nadol Jr JB (1988) Comparative anatomy of the cochlea and auditory nerve in mammals. Hear Res 34:253-266

Nadol Jr JB, Burgess BJ, Reisser C (1990) Morphometric analysis of normal human spiral ganglion cells. Ann Otol Rhinol Laryngol 99:340-348

Nadol Jr JB (1990) Degeneration of cochlear neurons as seen in the spiral ganglion of man. Hear Res 49:141-154

Paintal AS (1965) Effects of temperature on conduction in single vagal and saphenous myelinated nerve fibres of the cat. J Physiol (Lond) 180:20-49

Paintal AS (1966) The influence of diameter of medullated nerve fibres of cats on the rising and falling phases of the spike and its recovery. J Physiol (Lond) 184:791-811

Rattay F (1990) Electrical nerve stimulation: theory, experiments and applications. Springer Verlag, Wien New York

Rattay F, Aberham M (1993) Modeling axon membranes for functional electrical stimulation. IEEE Trans Biomed Eng 40:1201-1209

Rattay F, Lutter P, Felix H (2001) A model of the electrically excited human cochlear neuron I. Contribution of neural substructures to the generation and propagation of spikes. Hear Res 153:43-63

Reid G, Bostock H, Schwarz JR (1993) Quantitative description of action potentials and membrane currents in human node of Ranvier. J Physiol (Lond) 467:247P

Reid G, Scholz A, Bostock H, Vogel W (1999) Human axons contain at least five types of voltage-dependent potassium channel. J Physiol (Lond) 518:681-696

Reid MA, Flores-Otero J, Davis RL (2004) Firing Patterns of Type II Spiral Ganglion Neurons *In Vitro*. J Neurosci 24:733-742

Rosbe KW, Burgess BJ, Glynn RJ, Nadol Jr JB (1996) Morphologic evidence for three cell types in the human spiral ganglion. Hear Res 93:120-127

Rubinstein JT (1995) Threshold fluctuations in an *N* sodium channel model of the node of Ranvier. Biophys J 68:779-785

Rubinstein JT, Miller CA, Mino H, Abbas PJ (2001) Analysis of monophasic and biphasic electrical stimulation of nerve. IEEE Trans Biomed Eng 48:1065-1070

Schalow G, Zach GA, Warzok R (1995) Classification of human peripheral nerve fibre groups by conduction velocity and nerve fibre diameter is preserved following spinal cord lesion. J Auton Nerv Syst 52:125-150

Scherer SS, Arroyo EJ (2002) Recent progress on the molecular organization of myelinated axons. J Periph Nerv Sys 7:1-12

Scholz A, Reid G, Vogel W, Bostock H (1993) Ion channels in human axons. J Neurophysiol 70:1274-1279

Schwarz JR, Eikhof G (1987) Na currents and action potentials in rat myelinated nerve fibres at 20 and 37 °C. Pflügers Arch 409:569-577

Schwarz JR, Glassmeier G, Cooper EC, Kao T-C, Nodera H, Tabuena D, Kaji R, Bostock H (2006) KCNQ channels mediate IKs, a slow K^+ current regulating excitability in the rat node of Ranvier. J Physiol (Lond) 573:17-34

Schwarz JR, Reid G, Bostock H (1995) Action potentials and membrane currents in the human node of Ranvier. Pflügers Arch - Eur J Physiol 430:283-292

Shannon RV (1989) A model of threshold for pulsatile electrical stimulation of cochlear implants. Hear Res 40:197-204

Smit JE (2008) Modelled response of the electrically stimulated human auditory nerve fibre. Ph.D. thesis. University of Pretoria, Pretoria

Smit JE, Hanekom T, Hanekom JJ (2009) Modelled temperature-dependent excitability behaviour of a single Ranvier node for a human peripheral sensory nerve fibre. Biol Cybern 100:49-58

Smit JE, Hanekom T, Hanekom JJ (2008) Predicting action potential characteristics of human auditory nerve fibres through modification of the Hodgkin-Huxley equations. S Afr J Sci 104:284-292

Stephanova DI, Daskalova M, Alexandrov AS (2005) Differences in potentials and excitability properties in simulated cases of demyelinating neuropathies. Part I. Clin Neurophysiol 116:1153-1158

Taylor JT, Burke D, Heywood J (1992) Physiological evidence for a slow K^+ conductance in human cutaneous afferents. J Physiol (Lond) 453:575-589

Vabnick L, Trimmer JS, Schwarz TL, Levinson SR, Risal D, Shrager P (1999) Dynamic potassium channel distributions during axonal development prevent aberrant firing patterns. J Neurosci 19:747-758

Waxman SG (2000) The neuron as a dynamic electrogenic machine: Modulation of sodium-channel expression as a basis for functional plasticity in neurons. Phil Trans R Soc Lond B 355:199-213

Weiss G (1901) Sur la possibilité de rendre comparables entre eux les appareils servant a l'excitation électrique. Arch Ital Biol 35:413-446

Wesselink WA, Holsheimer J, Boom HBK (1999) A model of the electrical behaviour of myelinated sensory nerve fibres based on human data. Med Biol Eng Comput 37:228-235

White JA (2002) Action potential. In: Ramachandran VS (ed) Encyclopedia of the human brain, Academic press, Amsterdam, Boston, pp 1-12

Zhang X, Heinz MG, Bruce IC, Carney LH (2001) A phenomenological model for the responses of auditory-nerve fibers: I. Nonlinear tuning with compression and suppression. J Acoust Soc Am 109:648-670

Zimmermann CE, Burgess BJ, Nadol Jr JB (1995) Patterns of degeneration in the human cochlear nerve. Hear Res 90:192-201

Table 1. Parameters used for calculation of the voltage-dependent opening and closing rates of the ion channels. The transient sodium current activation parameters are subscripted with a '*t*' and the persistent sodium current activation parameters by a '*p*'.

Parameter	**Q_{10}**	**T_0 (°C)**	**A**	**B**	**C**	**D**
α_{mt}	2.16	20	4.42	2.5	0.1	1
β_{mt}	2.16	20	4.42	4.0	18	-
α_{h}	1.5	20	1.47	0.07	20	-
β_{h}	1.5	20	1.47	3.0	0.1	-
α_{ns}	1.5	20	0.2	1.0	0.1	10
β_{ns}	1.5	20	0.2	0.125	80	-
α_{mp}	1.99	20	2.06	2.5	0.1	1
β_{mp}	1.99	20	2.06	4.0	18	-

Table 2. Model electrical parameters

Parameter	Value	Q_{10}	T_0 (°C)	Reference
Membrane resting potential (V_{rest})	-79.4 mV	1.0356 for all T ≤ 20°C 1.0345 for all T > 20°C	6.3	(Hodgkin and Huxley 1952; Schwarz et al. 1995; Wesselink et al. 1999) †
Gas constant (R)	8.3145 J/K.mol			(Atkins 1995)
Faraday constant (F)	9.6485×10^4 C/mol			(Atkins 1995)
$[Na^+]_o/[Na^+]_i$	7.2102			(Hodgkin and Huxley 1952; Schwarz et al. 1995; Wesselink et al. 1999; Hille 2001) #
$[K^+]_o/[K^+]_i$	0.0361			(Scholz et al. 1993; Schwarz et al. 1995; Reid et al. 1999)
$[Leakage]_o/[Leakage]_i$	0.036645			(Scholz et al. 1993; Schwarz et al. 1995) ††
Sodium conductance (g_{Na})	640.00 mS/cm^2	1.02	24	(Scholz et al. 1993; Hille 2001)
Potassium conductance (g_K)	60.0 mS/cm^2	1.16	20	(Scholz et al. 1993; Schwarz et al. 1995; Reid et al. 1999) ††
Leakage conductance (g_L)	57.5 mS/cm^2	1.418	24	(Schwarz and Eikhof 1987; Scholz et al. 1993; Schwarz et al. 1995) ††
Axoplasmic (intracellular) resistivity (ρ_{ax})	0.025 kΩ.cm	$(1.35)^{-1}$	37	(Wesselink et al. 1999) †
Membrane capacitance (c_{mem})	2.8 μF/cm^2			(Schwarz et al. 1995) *
Myelin membrane capacitance (c_{my})	0.6 μF/cm^2			(Blight 1985)
Membrane resistance (R_{mem})	4.8707×10^4 Ω.cm^2	$(1.3)^{-1}$	25	(Blight 1985) †
Myelin membrane resistance (R_{my})	104 Ω.cm^2	$(1.3)^{-1}$	25	(Blight 1985) †

† Value deduced from reference(s) and then optimised for model. Q_{10} value not from reference, but optimised for model

Discrepancy exists between HH model value and values for human. Value hence optimised for model

†† Values deduced from reference(s) and corrected for concentration and temperature differences

* Considered constant for temperatures between 20 and 42°C

Table 3. Simulated rise and fall times for a 15.0 μm diameter general human peripheral sensory nerve fibre cable model compared to experimentally estimated results from human peripheral nerve fibres.

Parameter	**Specifications (15.0 μm fibre diameter)**	**Value**		
		Human peripheral nerve fibre model	**Experimental results**	**Reference**
Rise time (μs)	20°C	269	270	(Schwarz et al. 1995)
	25°C	203	204	(Schwarz et al. 1995)
	37°C	115	120	(Wesselink et al. 1999)
Fall time (μs)	20°C	1840	1829	(Schwarz et al. 1995)
	25°C	1424	1464	(Schwarz et al. 1995)
	37°C	754	470	(Wesselink et al. 1999)

Table 4. Simulated temperature dependency of conduction velocity and ARP and RRP for a general human peripheral sensory nerve fibre of about 13.0 μm diameter. Experimentally estimated results from Lowitzsch et al. (1977) are indicated in parenthesis for comparison.

Parameter	**Temperature (°C)**				**Q_{10} value**		**Reference**
	20	**25**	**30**	**35**	**30 - 20**	**35 - 25**	
Conduction velocity ($m.s^{-1}$)	28.81 (29.65)	36.52 (36.18)	42.35 (42.72)	46.20 (49.26)	1.47 (1.44)	1.27 (1.36)	(Lowitzsch et al. 1977)
ARP (ms)	2.30 (3.07)	1.70 (1.72)	1.30 (1.02)	1.00 (0.54)	$(1.77)^{-1}$ $((3.01)^{-1})$	$(1.70)^{-1}$ $((3.18)^{-1})$	(Lowitzsch et al. 1977)
RRP (ms)	20.40 (20.09)	10.30 (10.23)	5.10 (5.76)	3.16 (3.19)	$(4.00)^{-1}$ $((3.49)^{-1})$	$(3.23)^{-1}$ $((3.21)^{-1})$	(Lowitzsch et al. 1977)

Figure captions

Fig. 1. Representation of the generalised human peripheral sensory nerve fibre. The cable model consisted of a myelinated axon with 23 nodes separated by 22 internodes. Each node had a length of 1.061 μm and diameter d_{node}. The internodal axolemmal diameter (d_a) and internodal length depended on the total internodal nerve fibre diameter (d_f). The myelinated internodes were considered to be single cable structures as modelled by Blight (1985). In the equivalent circuit diagram the resistances and capacitances of the leaky myelin sheath (R_{my}, c_{my}) and axolemma (R_{mem}, c_{mem}) were combined together in series to form one compartment. The axoplasmic resistance (R_{ax}) was a function of the axoplasmic resistivity. The nodal circuit consisted of the axolemmal (membrane) resistance (R_{mem}) and capacitance (c_{mem}), as well as expressions for the sodium (g_{Na}), potassium (g_K) and leakage (g_L) conductances and equilibrium potentials (E_{Na}, E_K, E_L). The total nodal sodium current (I_{Na}) was subdivided into a 2.5% persistent (I_{Nap}) and 97.5% transient (I_{Nat}) sodium currents.

Fig. 2. Propagating AP for a 15.0 μm fibre plotted at 20°C. The fibre was externally stimulated with a monopolar electrode. The stimulating pulse was square, monophasic and anodic and 0.5 ms in duration. Only nodal APs are shown. Internodal APs were similar in nature than nodal APs.

Fig. 3. Relationship between AP rise and fall times and fibre diameter plotted at 25°C and 37°C.

a. AP rise times decreased as the temperature was increased. They increased with a decrease in fibre diameter down to 7.5 μm and then decreased for thinner fibres.

b. AP fall times were longer at lower temperatures compared to higher temperatures. Fall times decreased with a decrease in fibre diameter down to 10.0 μm and increased for thinner fibres.

Fig. 4. Influence of different nerve fibre cable model parameters on the AP duration, plotted against fibre diameter at 25°C.

a. AP rise times were similar for nerve fibre models containing only a transient sodium (I_{Nat}) current and containing both a transient (I_{Nat}) and persistent (I_{Nap}) sodium currents respectively. With the latter model, an increase in the axonal diameter did not influence the rise times. Equating the nodal diameter to the axonal diameter, i.e. ignoring nodal strangulation, resulted in rise times displaying almost no fibre dependence.

b. Comparison of AP fall times for same parameters as in **a.** AP fall times decreased in the cases of a model containing only a transient sodium (I_{Nat}) current and an increase in the axonal diameter respectively. Similar to rise times, fall times also displaying almost no fibre dependence when nodal strangulation was ignored.

c. AP rise times increased, but followed the same trend for different axoplasmic resistivity (ρ_{ax}) values of 0.025 kΩ.cm (continuous line; circles), 0.033 kΩ.cm (dashed line; upright triangles) and 0.07 kΩ.cm (dash-dot-dot line; upside down triangles) respectively and a Q_{10} factor of $(1.35)^{-1}$.

d. AP fall times decreased, but followed the same trend when using the same ρ_{ax} values as in **c.**

Fig. 5. AP duration plotted against fibre diameter. For fibre diameters larger than 7.5 μm, AP duration showed an inverse relationship to fibre diameter at temperatures higher than 27°C. At lower temperatures durations increased again for fibres larger than 12.5 μm.

Fig. 6. Temperature dependence of normalised AP durations plotted for fibre diameters larger than 7.5 μm. These results were obtained from curves similar to and including the curves in Figs. 3 and 5. Results were normalised to AP durations at 37°C. Curve slopes indicated a faster increase in AP duration for thicker fibres.

Fig. 7. AP duration Q_{10} factors for temperature ranges 20 to 27°C and 27 to 37°C respectively, plotted against fibre diameter. Q_{10} factors were calculated from the curves in Fig. 6. For fibre diameters larger than 7.5 μm, Q_{10} factors of the higher temperature range increased faster with a fibre diameter increase compared to the lower temperature range, indicating a change in AP duration slope in all fibres at 27°C.

Fig. 8. Conduction velocity plotted against fibre diameter (continuous line; open circles). Simulations were performed at 37°C. Experimental data from Schalow et al. (1995) (dashed line; closed circles) and simulation data from Wesselink et al. (1999) (dash-dot line).

Fig. 9. Conduction velocity plotted against fibre diameter for different axoplasmic resistivity (ρ_{ax}) values of 0.025 kΩ.cm (continuous line; circles), 0.033 kΩ.cm (dashed line; upright triangles) and 0.07 kΩ.cm (dash-dot-dot line; upside down triangles) respectively and a Q_{10} factor of $(1.35)^{-1}$. Curves predicted with a Q_{10} factor of $(1.30)^{-1}$ were similar to the curves shown and were omitted for clarity. Simulations were performed at 37°C.

Fig. 10. Chronaxie time constant plotted against fibre diameter for a simulated nerve fibre containing 2.5% persistent (I_{Nap}) and 97.5% transient (I_{Nat}) sodium currents including (long dashed line) and excluding (short dashed line) nodal strangulation. Simulation temperature was 37°C. Chronaxie time results for a nerve fibre similar to the general sensory nerve fibre, but containing only a transient (I_{Nat}) sodium current, reproduced from Smit et al. (2008) (dash-dot-dot line). Results from Wesselink et al. (1999) model reproduced for comparison purposes (solid line).

Fig. 11. Chronaxie time constant plotted against temperature for a simulated nerve fibre containing a 2.5% persistent (I_{Nap}) and 97.5% transient (I_{Nat}) sodium currents including (long dashed line) and excluding (short dashed line) nodal strangulation. Simulation temperature was 37°C. Chronaxie time results for a nerve fibre similar to the general sensory nerve fibre, but containing only a transient (I_{Nat}) sodium current (dash-dot-dot line), included for comparison.

Figure 1

Click here to download high resolution image

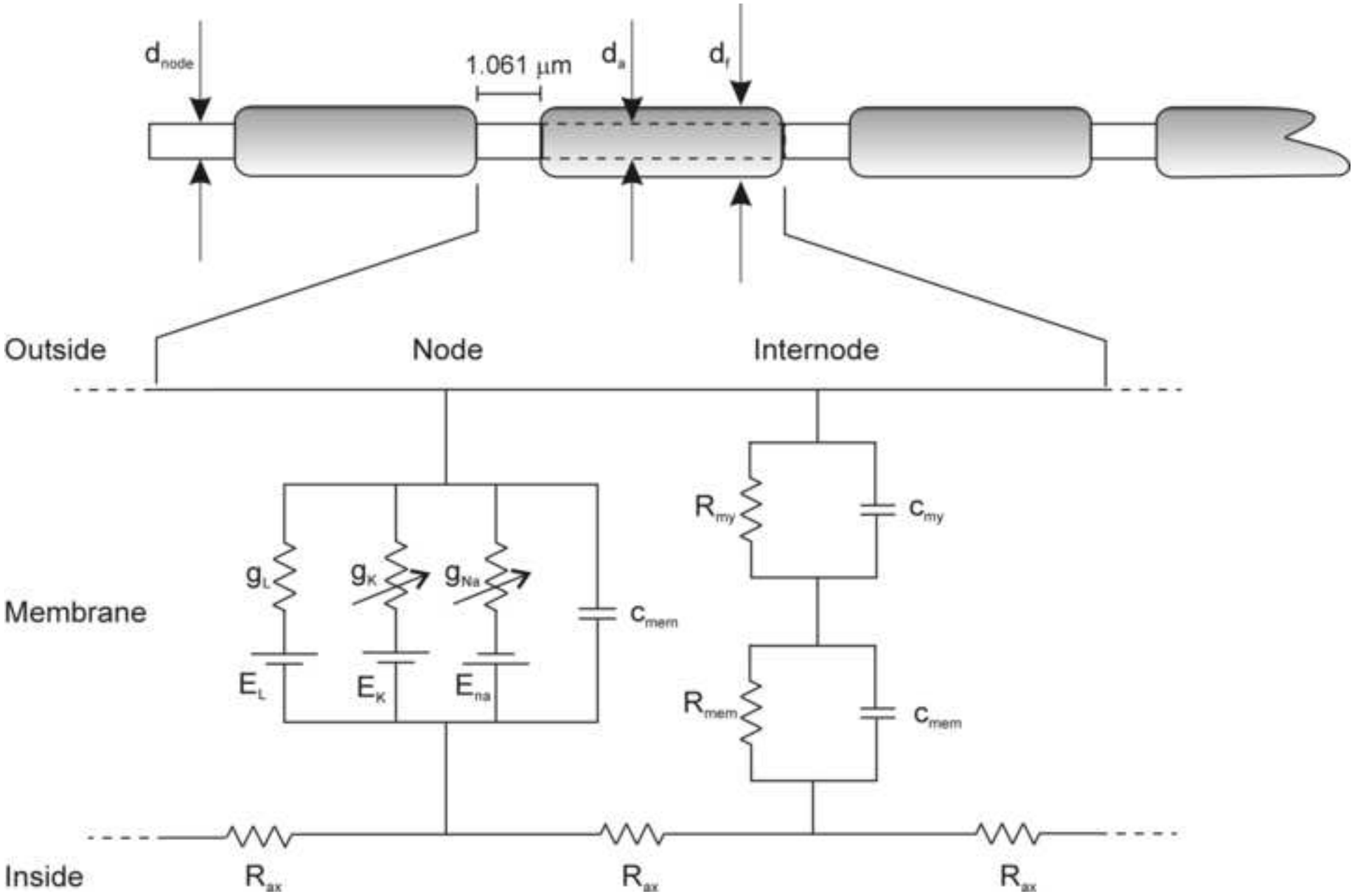

Figure 2

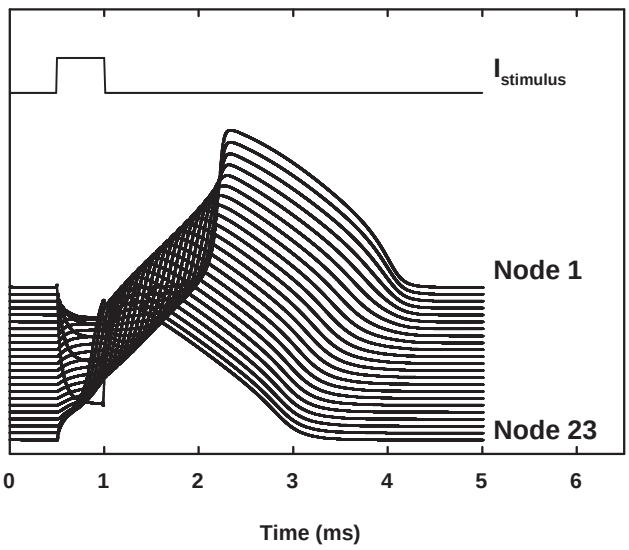

Figure 3

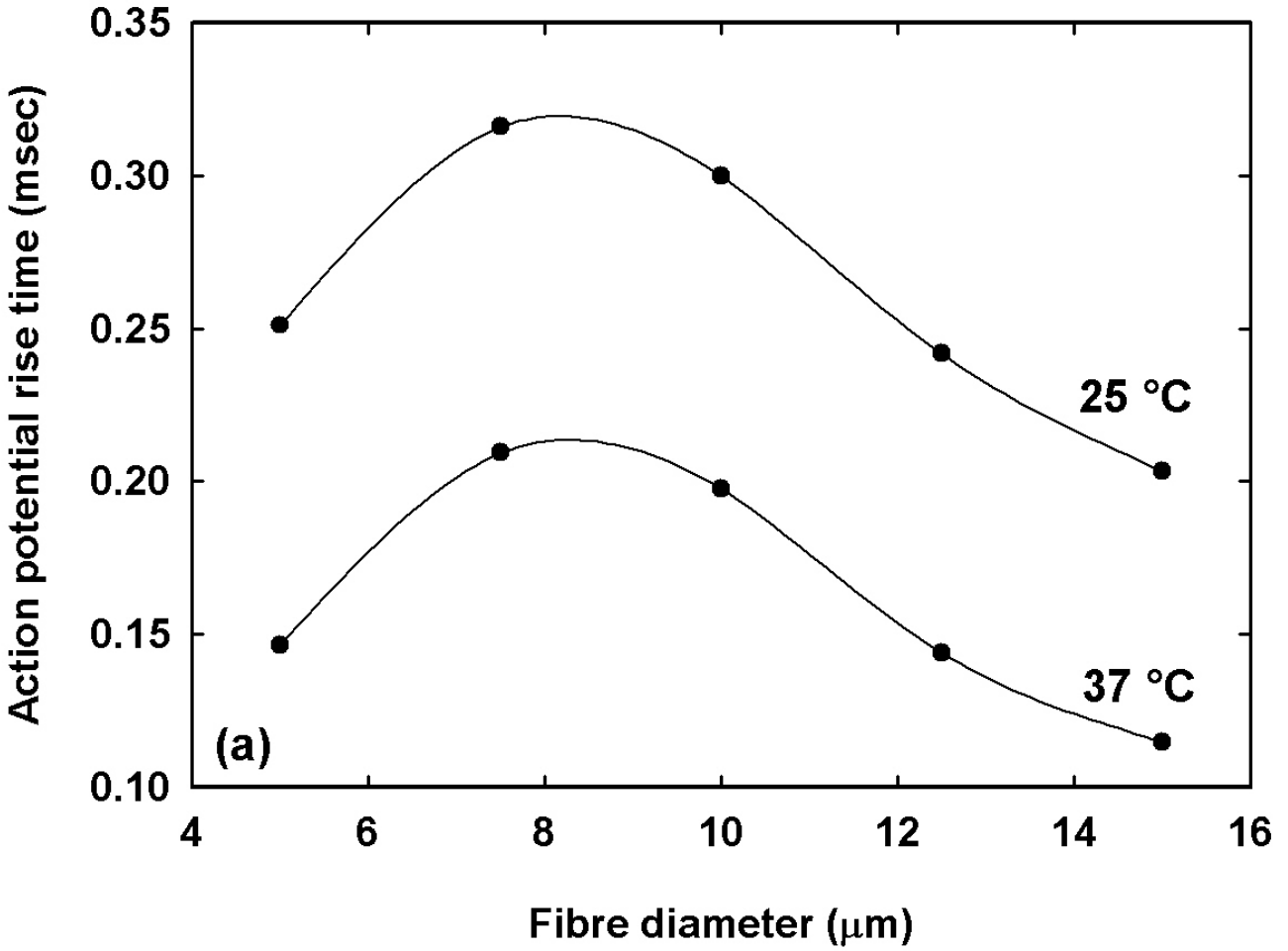
0.35
0.30
0.25
0.20
0.15
0.10
Action potential rise time (msec)
25 °C
37 °C
(a)
4
6
8
10
12
14
16
Fibre diameter (μm)

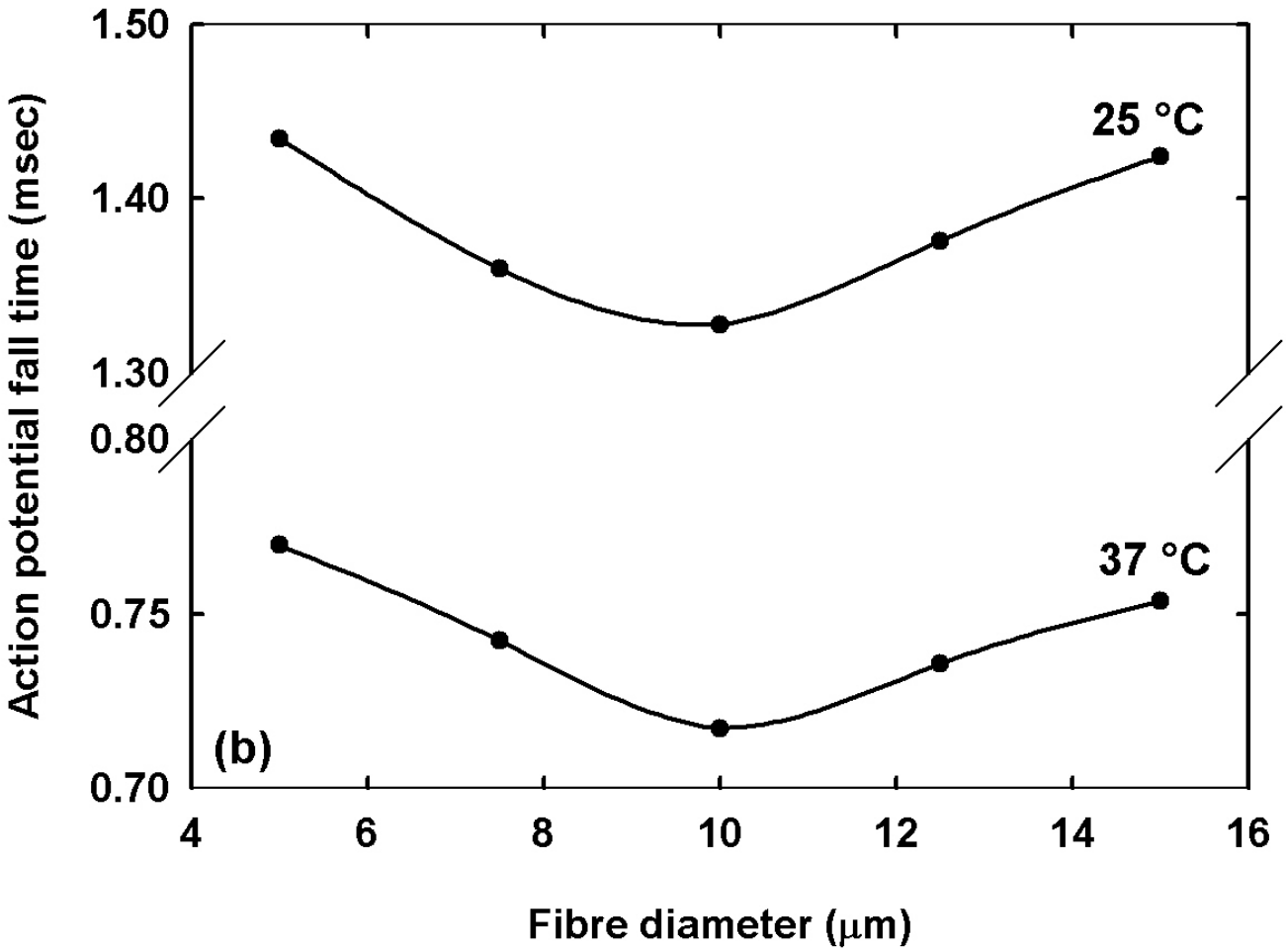
1.50
1.40
1.30
0.80
0.75
0.70
Action potential fall time (msec)
25 °C
37 °C
(b)
4
6
8
10
12
14
16
Fibre diameter (μm)

Figure 4

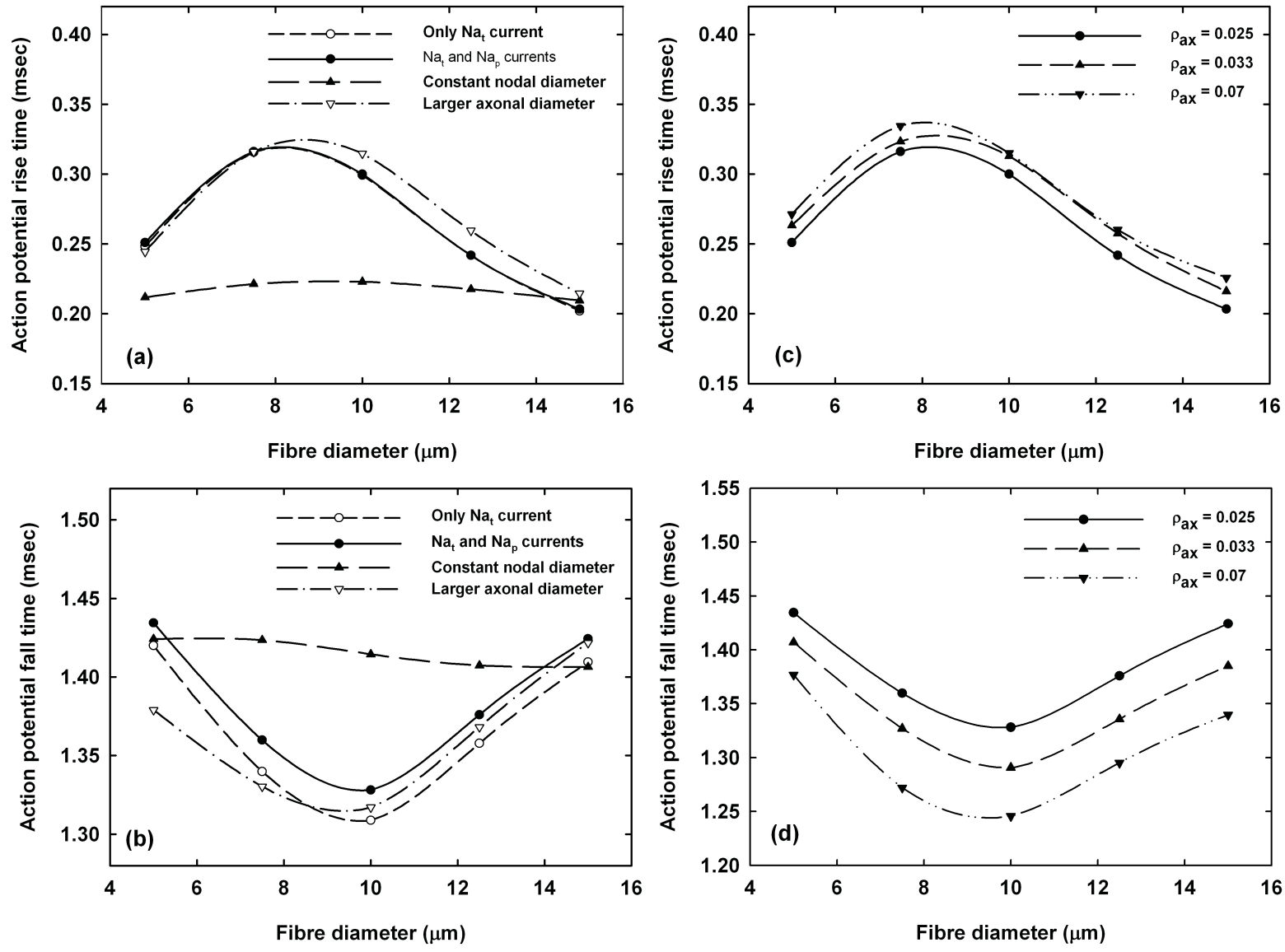
Only Na_t current
Na_t and Na_p currents
Constant nodal diameter
Larger axonal diameter
Action potential rise time (msec)
Fibre diameter (μm)
(a)
ρ_{ax} = 0.025
ρ_{ax} = 0.033
ρ_{ax} = 0.07
(c)
Action potential fall time (msec)
(b)
(d)

Figure 5

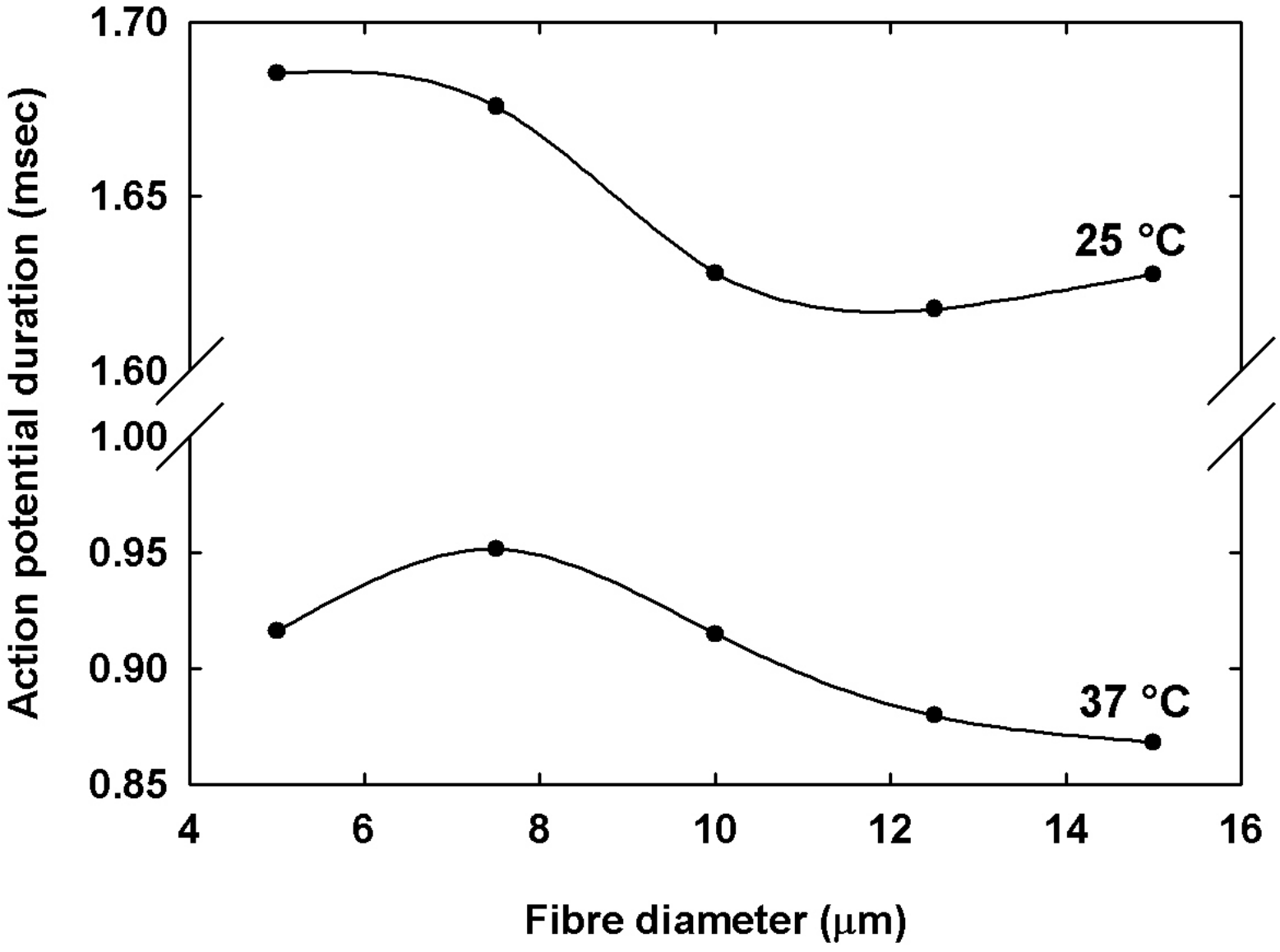
1.70
1.65
1.60
1.00
0.95
0.90
0.85
25 °C
37 °C
Action potential duration (msec)
4
6
8
10
12
14
16
Fibre diameter (μm)

Figure 6

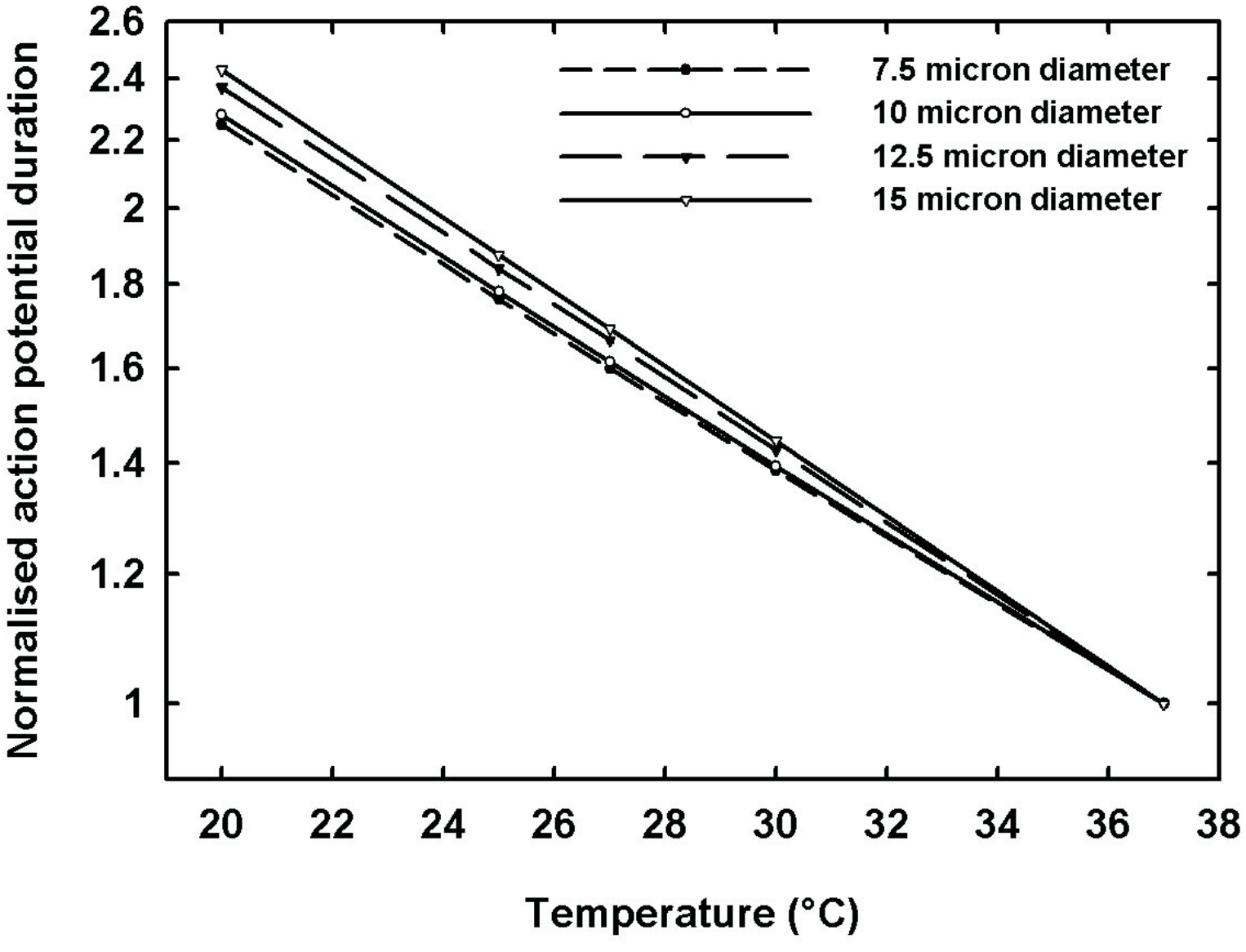
Normalised action potential duration
2.6
2.4
2.2
2
1.8
1.6
1.4
1.2
1
20
22
24
26
28
30
32
34
36
38
Temperature (°C)
7.5 micron diameter
10 micron diameter
12.5 micron diameter
15 micron diameter

Figure 7

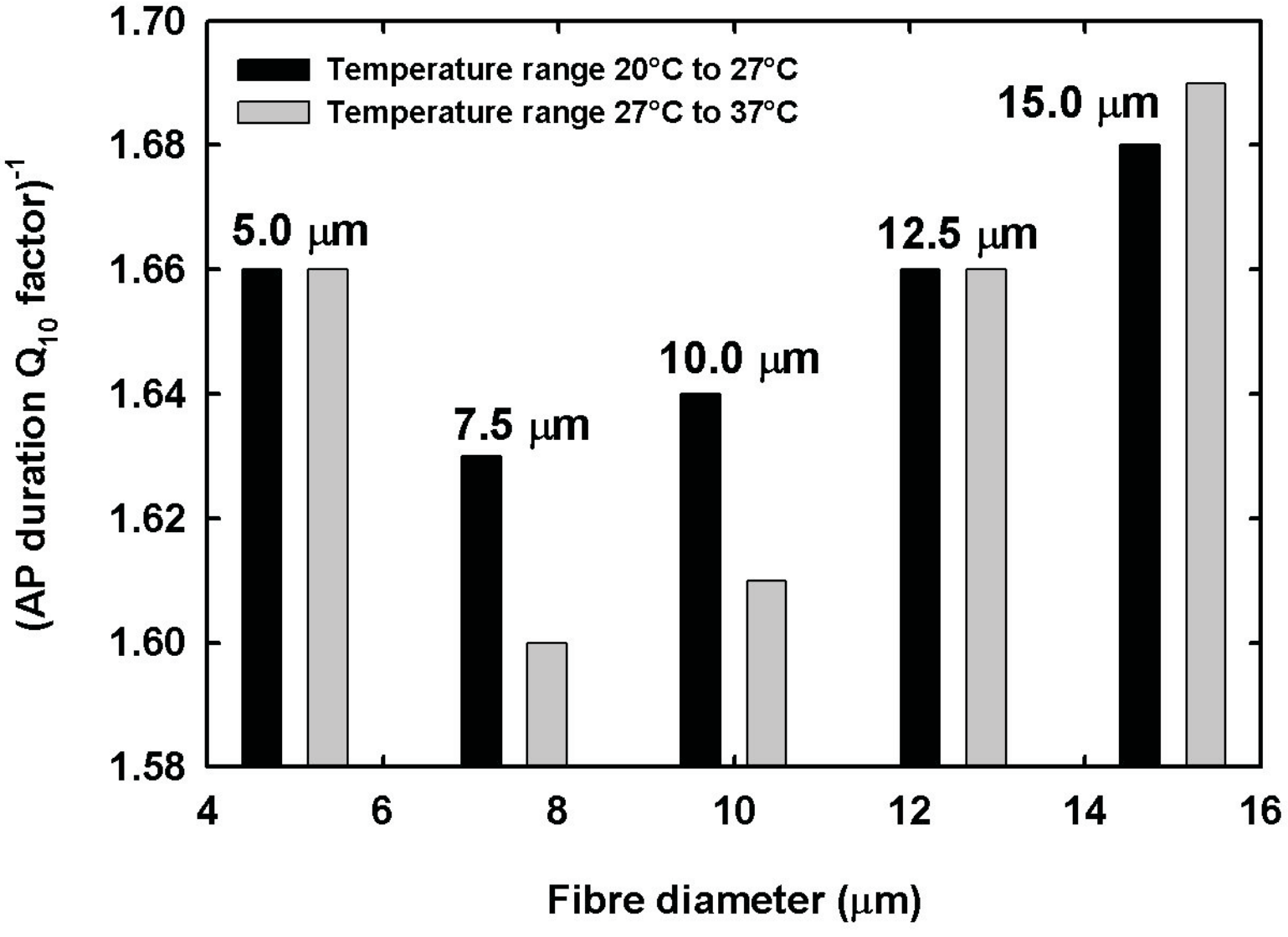
Temperature range 20°C to 27°C
Temperature range 27°C to 37°C
5.0 μm
7.5 μm
10.0 μm
12.5 μm
15.0 μm
(AP duration Q10 factor)-1
1.70
1.68
1.66
1.64
1.62
1.60
1.58
4
6
8
10
12
14
16
Fibre diameter (μm)

Figure 8

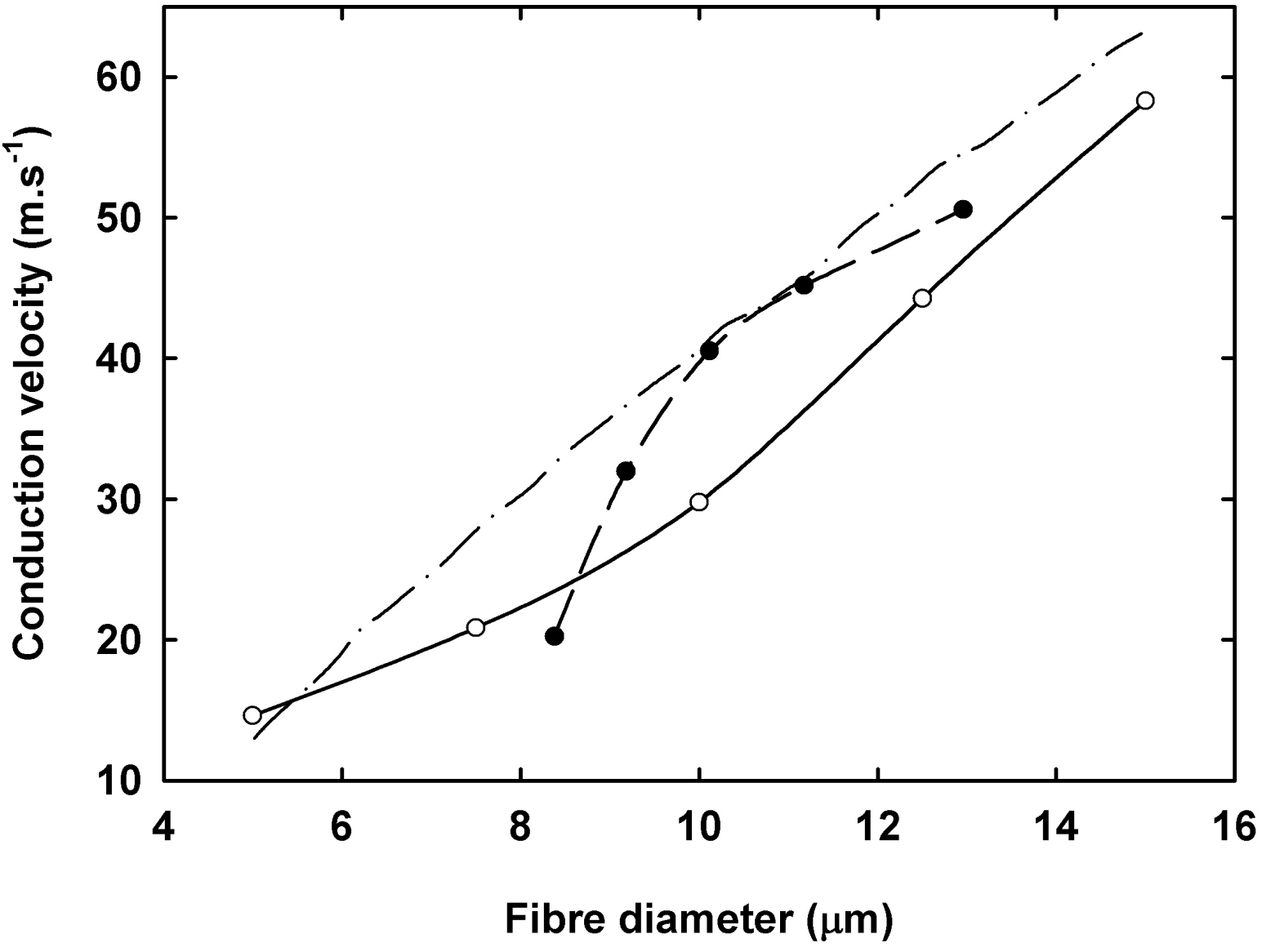
Conduction velocity (m.s-1)
60
50
40
30
20
10
4
6
8
10
12
14
16
Fibre diameter (μm)

Figure 9

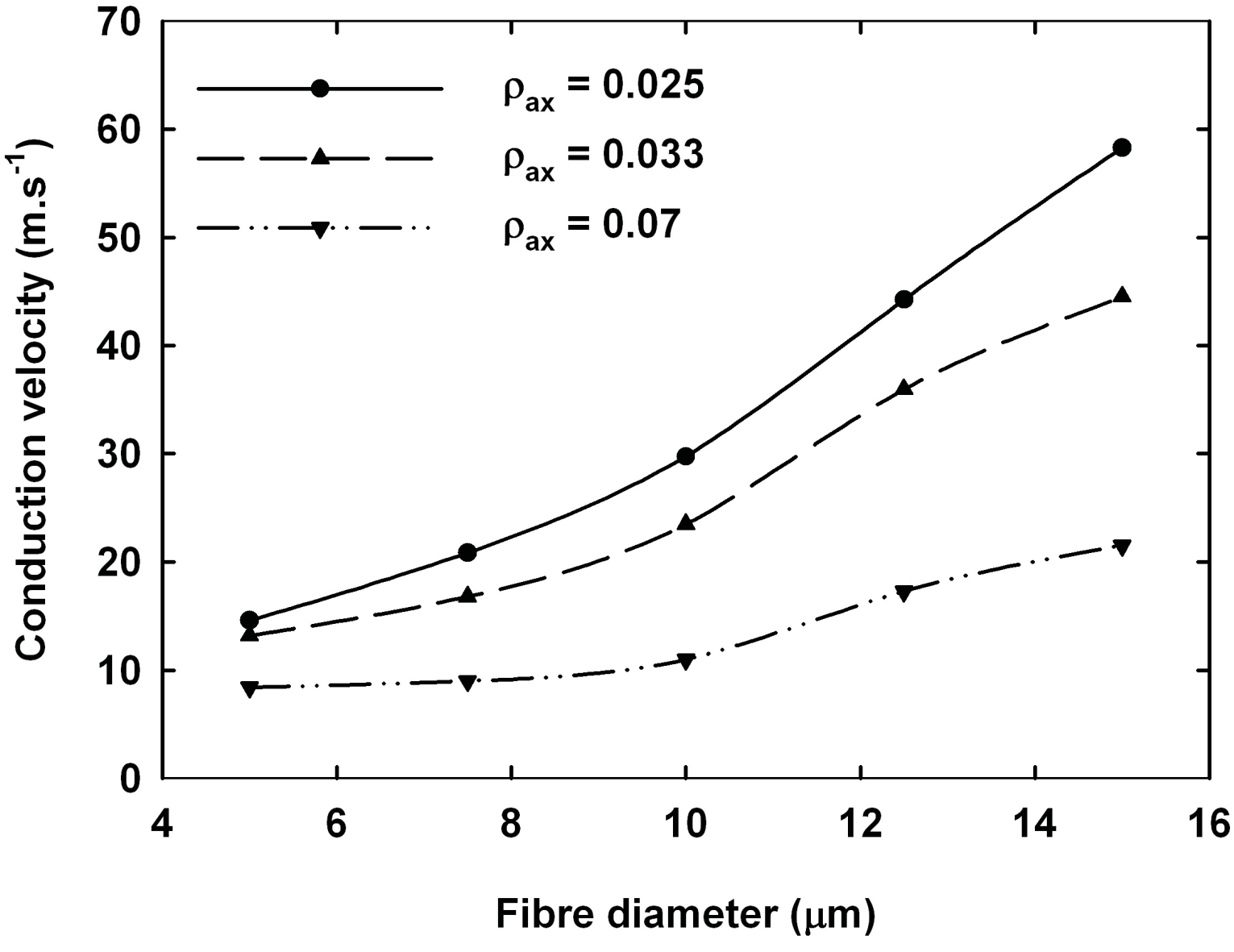
70
60
50
40
30
20
10
0
4
6
8
10
12
14
16
Conduction velocity (m.s-1)
Fibre diameter (μm)
ρax = 0.025
ρax = 0.033
ρax = 0.07

Figure 10

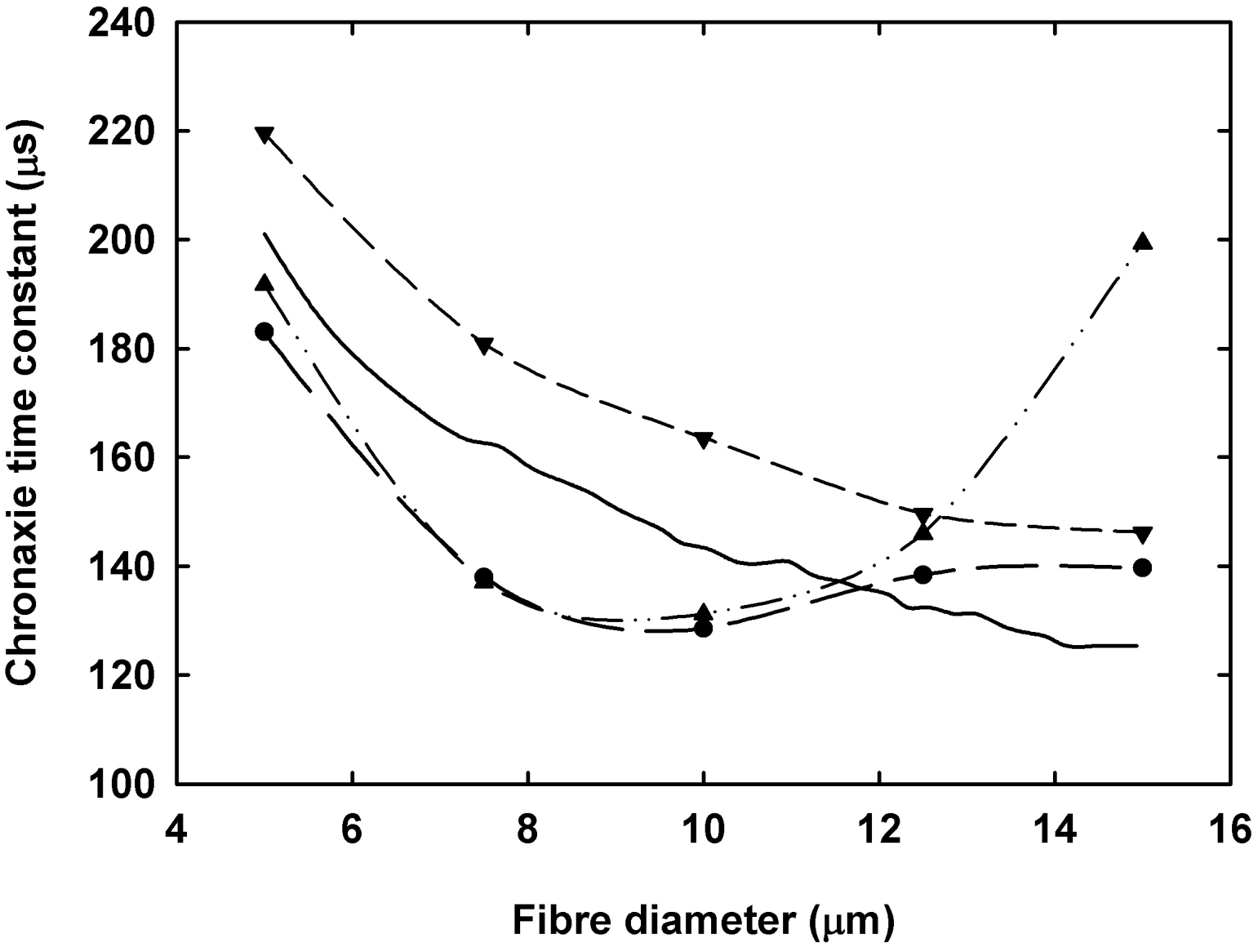
240
220
200
180
160
140
120
100
Chronaxie time constant (μs)
4
6
8
10
12
14
16
Fibre diameter (μm)

Figure 11

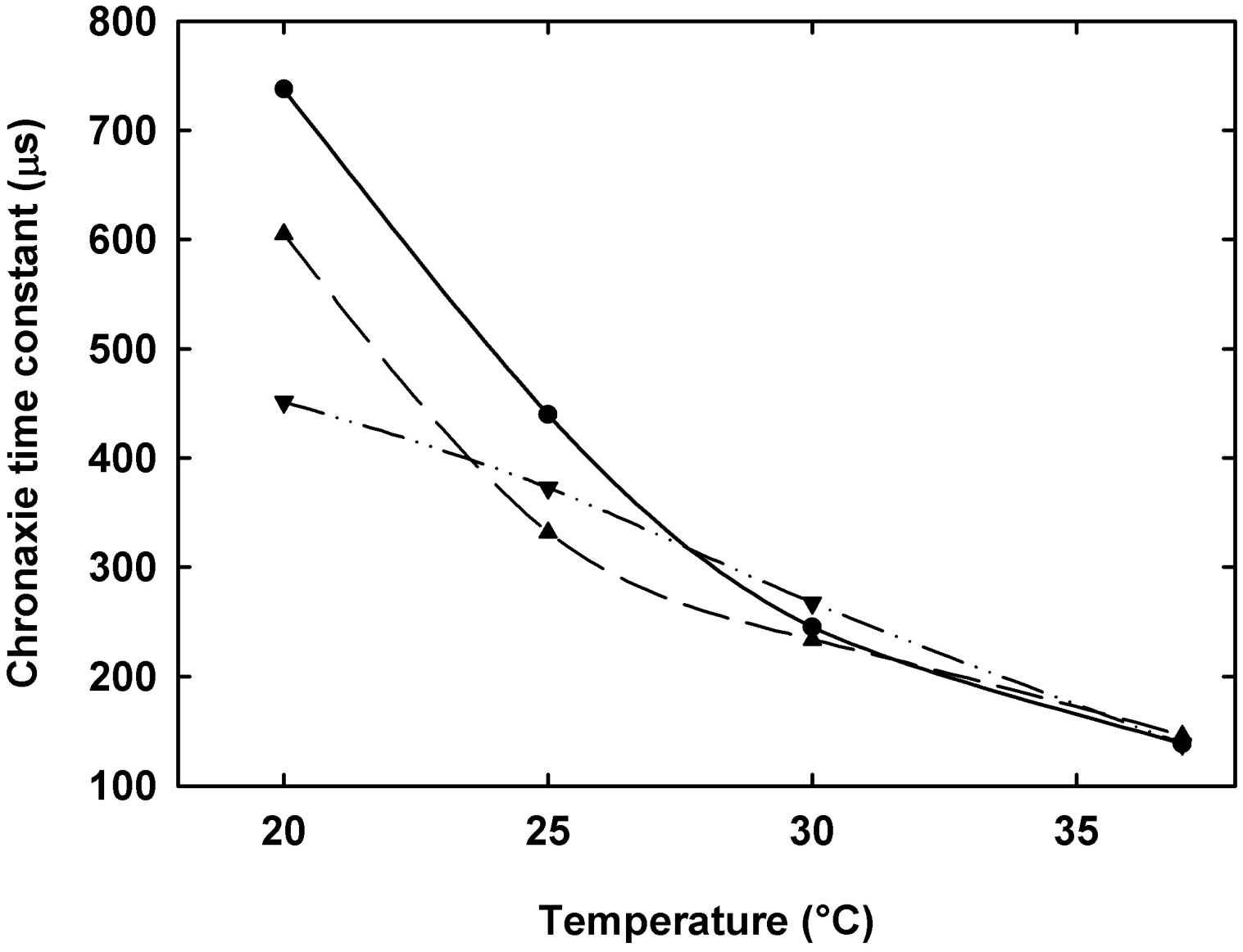
800
700
600
500
400
300
200
100
Chronaxie time constant (µs)
20
25
30
35
Temperature (°C)